Modeling plasma-based CO_2 and CH_4 conversion in Mixtures with N_2, O_2, and H_2O : the bigger plasma chemistry picture

Modeling Plasma-based CO_2 and CH_4 Conversion in Mixtures with N_2, O_2 and H_2O: the Bigger Plasma Chemistry Picture

Weizong Wang*[, 1, (a)], Ramses Snoeckx*[, 1, 2, (a)], Xuming Zhang[2, 3], Min Suk Cha[2] and Annemie Bogaerts*[,1]

1. Research group PLASMANT, Department of Chemistry, University of Antwerp, Universiteitsplein 1, B-2610 Wilrijk-Antwerp, Belgium

2. King Abdullah University of Science and Technology (KAUST), Clean Combustion Research Center (CCRC), Thuwal 23955, Saudi Arabia

3. College of Environmental Science and Engineering, Zhejiang Gongshang University, Xiasha High Education District, Hangzhou, Zhejiang Province, China

Corresponding Author

*E-mail: wangweizong@gmail.com , ramses.snoeckx@uantwerpen.be , annemie.bogaerts@uantwerpen.be

(a) These authors contributed equally to this work

ABSTRACT: Due to the unique properties of plasma technology, its use in gas conversion applications is gaining significant interest around the globe. Plasma-based CO_2 and CH_4 conversion have become major research areas. Many investigations have already been performed regarding the single component gases, i.e. CO_2 splitting and CH_4 reforming, as well as for two component mixtures, i.e. dry reforming of methane (CO_2/CH_4), partial oxidation of methane (CH_4/O_2), artificial photosynthesis (CO_2/H_2O), CO_2 hydrogenation (CO_2/H_2), and even first steps towards the influence of N_2 impurities have been taken, i.e. CO_2/N_2 and CH_4/N_2. In this feature article we briefly discuss the advances made in literature for these different steps from a plasma chemistry modeling point of view. Subsequently, we present a comprehensive plasma chemistry set, combining the knowledge gathered in this field so far, and supported with extensive experimental data. This set can be used for chemical kinetics plasma modeling for all possible combinations of CO_2, CH_4, N_2, O_2 and H_2O, to investigate the bigger picture of the underlying plasmachemical pathways for these mixtures in a dielectric barrier discharge plasma. This is extremely valuable for the optimization of existing plasma-based CO_2 conversion and CH_4 reforming processes, as well as for investigating the influence of N_2, O_2 and H_2O on these processes, and even to support plasma-based multi-reforming processes.

Submitted as invited feature article to The Journal of Physical Chemistry C

1. INTRODUCTION: PLASMA TECHNOLOGY

Today—more than ever—plasma technology lies at the base of modern technology, as the entire microelectronics industry relies on plasma-surface interactions. [1-2] These interactions make it possible for scientists to extend Moore's law by providing the current nanometer resolution of microprocessors.

In general, plasma consists of various types of ions (both positive and negative), electrons and a large variety of neutral species, i.e. different types of atoms, molecules, radicals and excited species. This makes plasma a highly reactive—but complex—chemical cocktail, which is of interest to many potential applications.[1,3-4]

Plasma is often referred to as the 'fourth state of matter'. Indeed, upon increasing energy input, matter transforms in the sequence: solid, liquid, (neutral) gas and finally ionized gas or plasma. Although plasma might not be so widely known as the other three states of matter, 99 % of the visible universe is actually in plasma state, mainly as stars (including our Sun) and interstellar matter. Furthermore, natural plasmas also occur on Earth, in the form of most natural occurring weather phenomena which emit light, e.g. lightning, auroras (Borealis and Australis), Saint Elmo's fire, and red sprites.

Beside natural plasmas, two main groups of man-made plasmas are distinguished, i.e. high temperature or fusion plasmas and low temperature plasmas or gas discharges. The latter group can be further subdivided based on whether or not the plasma is in thermal equilibrium. Due to the multitude in different types of species, which can all have different temperatures and degrees of freedom, plasma can exhibit—and is defined by—multiple temperatures, e.g., gas temperature, electron temperature, ion temperature, vibrational temperature, rotational temperature. When—in a localized area—these temperatures are the same, the plasma is said to be in 'local thermodynamic equilibrium' (LTE), and mostly called a 'thermal plasma'. In the other case, the plasma is said to be in 'non-local thermodynamic equilibrium' (non-LTE), and mostly called a 'non-thermal plasma'.

One of the main reasons why low temperature (non-LTE) plasmas have such a large potential for a wide variety of applications, is their capability of producing a reactive chemical environment while staying at room temperature. This is possible due to most of the energy being directed into the electrons, leading to a much higher electron temperature (T_e), compared to the gas temperature (T_g). Subsequently, these highly energetic electrons can activate the gas and initiate reactions by electron impact collisions, rather than the classical form of energy used in industry, i.e. heat.

Applications range from materials science (e.g., coating deposition, surface modification, nanotechnology, and chip manufacturing, as mentioned above) over lighting, lasers, plasma displays (as plasma emits light due to the presence of many excited species), to analytical chemistry, thrusters, as well as environmental, energy and medical applications (e.g., sterilization, wound healing and even cancer treatment). [1,3-4] Environmental and energy applications include, among others, air pollution control, [5] nitrogen fixation from the air to form ammonia and nitric oxides, [6-7] hydrocarbon reforming [8-10] and CO_2 conversion into value-added chemicals and fuels. [11] These applications often use a combination of plasma with catalysts, yielding plasma catalysis.[11-14]

To improve these applications, a good knowledge of the underlying plasma processes is indispensable. The

latter can be obtained by experiments and computer modeling. As detailed measurements inside the plasma are not always straightforward, modeling can indeed be of great value. This feature article will focus on the continuous research efforts in modeling the plasma chemistry for the growing application of low temperature (non-LTE) plasmas used for CO_2 conversion and CH_4 reforming, as well as combinations with other gases, and highlight the contributions of the PLASMANT research group in this field.[15-16] Based on the gained knowledge so far, and an extensive set of experiments carried out for various gas mixtures and mixing ratios, a new comprehensive plasma chemistry model is presented that can be used to describe the underlying mechanisms of CO_2 and CH_4 conversion, also in the presence of N_2, O_2 and H_2O.

2. PLASMA CHEMISTRY MODELING FOR CO_2 CONVERSION AND CH_4 REFORMING

Interest in the application of plasma technology for CO_2 conversion and CH_4 reforming has been growing rapidly. [9,11,17-20] Due to the adverse effects of climate change on our society, the conversion of these gases into value-added chemicals and fuels is considered as one of the great challenges of the 21st century.[21] Successfully converting the greenhouse gas CO_2 would be interesting from both an economic and ecological perspective. This would lead to the successful generation of an artificial closed carbon loop, which fits into the 'cradle-to-cradle' concept,[22] i.e., upcycling waste material into new feedstock. Additionally, with the increase of biogas, landfill gas and hydrogenation of CO_2 to CH_4, the straightforward reforming of CH_4 into liquid products would be beneficial, because the energy density of liquid fuel is much higher and it is easier to transport.[23-24]

As outlined in an extensive recent review on the use of plasma technology for CO_2 conversion: [11] "Plasmas possess some important advantages over other (novel) technologies for the conversion of CO_2 and CH_4: (i) they can operate at room temperature using any source of (renewable) electricity, (ii) they have a large flexibility in terms of the feeds that need to be processed, (iii) they provide an extremely flexible 'turnkey' process, which allows for the efficient storage of energy, peak shaving and grid stabilization, (iv) the reactors have low investment and operating costs, (v) they have a simple scalability both in size and applicability, and (vi) last but not least, the technology does not rely on rare earth materials—making it rather unique at this point. This unprecedented combination of features gives plasmachemical conversion a very high overall flexibility, making it an extremely useful and valuable technology for CCU."

To improve this application, several research groups developed models for chemical kinetics simulations, to better understand the underlying mechanisms, and a brief literature overview will be given below. This development can be subdivided in three main stages: (1) modeling single component molecular gases, i.e. plasma-based CO_2 splitting and CH_4 reforming; (2) investigating common two component mixtures, i.e. dry reforming of methane (CO_2/CH_4), partial oxidation of methane (CH_4/O_2), artificial photosynthesis (CO_2/H_2O) and CO_2 hydrogenation (CO_2/H_2); (3) moving towards more realistic gas mixtures by investigating the effect of N_2 both as admixture and impurity, i.e. CO_2/N_2 and CH_4/N_2. The following subsections will be divided according to these three stages.

The knowledge obtained during these different stages is now combined into one comprehensive chemical kinetics plasma model for use in low temperature (non-LTE) plasmas, presented for the first time in this feature

article. Therefore, in the following subsections, we will each time compare the CO_2 and/or CH_4 conversion, calculated with this new model, with our previous (published) experimental data, in order to step-by-step validate the individual chemistry sets. This validation will be performed for a dielectric barrier discharge (DBD) plasma, as the chemistry model presented in this feature article is specifically developed for this type of plasma. A DBD plasma is created by applying a potential difference between two electrodes, of which at least one is covered by a dielectric barrier. For CO_2 and CH_4 conversion applications, a tubular DBD reactor is most often used,[11] consisting of an inner electrode surrounded by a dielectric tube, covered by an outer electrode (see Figure 1).

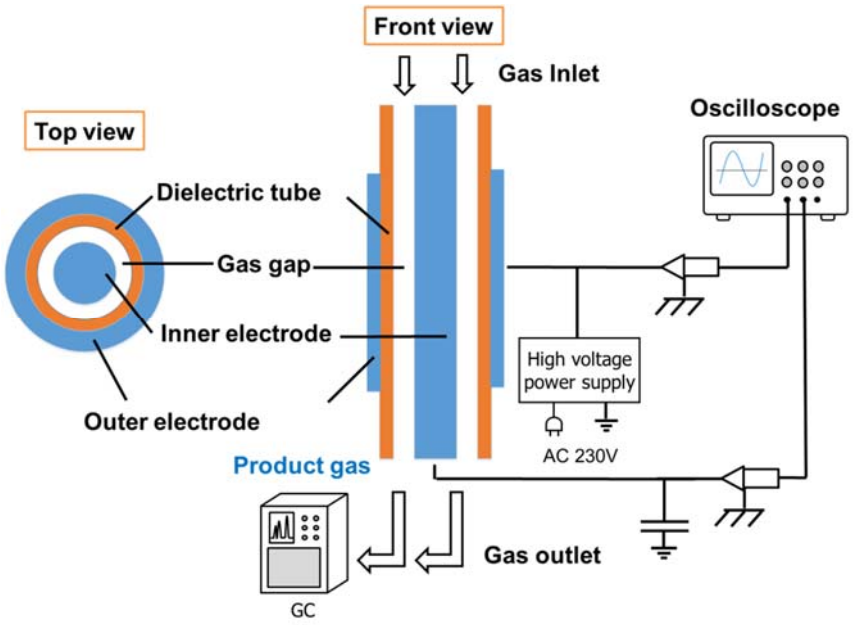

Figure 1. Schematic diagram of a dielectric barrier discharge (DBD).

Subsequently, in section 3 we will present this new comprehensive chemical kinetics plasma model for use in low temperature (non-LTE) plasmas. The applications of this extensive model are broad. They can range from very specific investigations, like the effect of CH_4 on NO_x mitigation for CO_2/N_2 plasmas, to realistic industrial gas mixtures for dry reforming of methane by inclusion of N_2, as well as unravelling the possibilities for plasma-based multi-reforming processes. Furthermore, this chemistry set can also be used as a foundation to build a comprehensive computational data set in the field of plasma-assisted combustion. [25-26] Finally, certain data from this set could even be used for exotic models, like planetary atmosphere and spacecraft re-entry modeling. [27-28]

2.1 Single Component Molecular Gases

With the breakthrough of sufficient—and continuously increasing—computational power available to researchers, plasmachemical modeling efforts could expand from simple noble gases towards reactive molecular gases.

In the past 10 years many different plasmachemical kinetic models have been developed for pure CO_2 splitting in various kinds of plasmas.[9,29-49] Several of these models have been developed in the research group

PLASMANT.[29-39] Furthermore, there is also interest in pure CH_4 reforming, also known as 'the pyrolysis of methane', used to synthesize higher hydrocarbons. [9] Few models exist in literature,[50-53] of which one has been developed in the research group PLASMANT. [52]

Figure 2 illustrates a comparison of the calculated CO_2 conversion, using our new comprehensive model (see section 3), with measured values for a pure CO_2 DBD plasma, [29] at a fixed plasma power of 40 W and varying the gas flow rate to yield different values of the specific energy input (SEI). The CO_2 conversion is mainly caused by electron impact dissociation at these conditions (see below and ref. (29)). The conversion gradually increases with rising SEI, both in the experiments and calculation results, which is logical as more energy is put into the system. Above 25 eV/molecule, the model does not show saturation yet, although it is observed in the experimental data. However, as described in the review of Snoeckx and Bogaerts,[11] these higher SEI values are not attractive, because of very low energy efficiency. The recommended SEI range is in the order of 0.1 to 5 eV/molecule. Therefore, we may conclude that the agreement between model and experiments is good, especially in the SEI region of most practical interest.

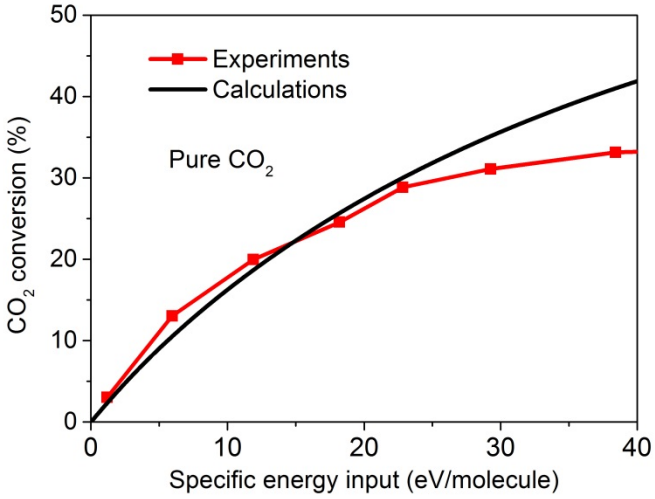

Figure 2. Comparison of the calculated CO_2 conversion, as obtained from our new comprehensive plasma chemistry model, with measured data adopted from ref. 29, as a function of SEI, at a fixed plasma power of 40 W and varying gas flow rate.

2.2 Two Component Mixtures

With even more computing power and the successful development of models for simulating single component molecular gases, as described above, the combination of these models into two component reactive mixtures was the logical—albeit not always easy—next step.

2.2.1 Dry Reforming and Partial Oxidation Of Methane

The combined conversion of CO_2 and CH_4, also known as 'dry reforming of methane' (DRM) has been extensively studied, [9,11] and a variety of models have been developed in literature. [54-66] Again, several of these models have been developed within the research group PLASMANT.[63-66] Besides CO_2, another—stronger—oxidant used to reform CH_4 is O_2, and this combination is known as 'partial oxidation of methane' (POX). [9]

Several modeling investigations exist in literature, [66-72] including one from our group PLASMANT. [66] Although this process leads to higher CH_4 conversions than DRM, its strong oxidative character causes a total oxidation of CH_4, producing CO_2, and is therefore of less interest.

Figure 3 illustrates the calculated absolute conversions of CH_4 and CO_2 in plasma-based DRM as a function of discharge power using our new comprehensive model (see section 3), in comparison with experimental values obtained from Ref. (63), for a DBD in a 1:1 CO_2/CH_4 mixture at a total flow rate of 50 sccm. The CH_4 and CO_2 conversions both increase with discharge power, which is again logical, and the CH_4 conversion is about a factor 1.5 higher than the CO_2 conversion. Very good agreement is reached between calculated and experimental conversions.

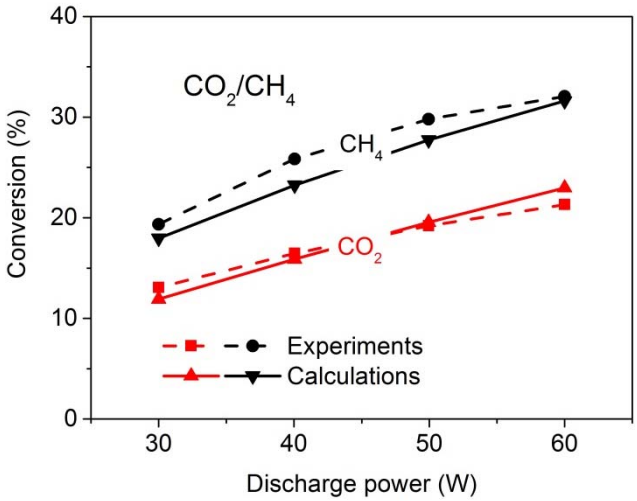

Figure 3. Comparison of the calculated absolute conversion of CO_2 and CH_4, as obtained from our new comprehensive plasma chemistry model, with measured data adopted from ref. (63), in a 1:1 CO_2/CH_4 mixture at a total flow rate of 50 sccm, as a function of discharge power.

2.2.2 Artificial Photosynthesis and CO_2 Hydrogenation

Research towards CO_2 conversion in the presence of H_2O (artificial photosynthesis) and H_2 (CO_2 hydrogenation) is quite limited and to our knowledge the only models available are developed within the research group PLASMANT. [73-74]

In figure 4, the calculated absolute CO_2 and H_2O conversions, as obtained from our new plasma chemistry model, are compared with experimental data for a DBD, as a function of water vapor content for a total gas flow rate of 600 mL/min at 323 K for a SEI value of 1.1 eV/molecule. Both the experimental and calculated absolute H_2O conversions show a slightly decreasing trend with increasing water vapor content, although the drop is more pronounced in the simulation results. This is probably due to some more complex processes taking place in the experiments as a result of water vapor, which could not be easily accounted for in the 0D plasma chemistry model. Indeed, the model does not take into account some physical effects, such as condensation and nebulization. [73] Furthermore, water cluster ions and surface processes, which might be important in a water discharge, [75] are not yet taken into account in our current model.

The experiments also show a slight drop in CO_2 conversion with increasing water content. As explained in Ref. (73), this may result from destabilization of the discharge induced by the presence of water. This trend is also not captured by the simulation, but the agreement is still reasonable, because both simulations and experiments show that the addition of water vapor into CO_2 only exerts a weak influence on the CO_2 conversion.

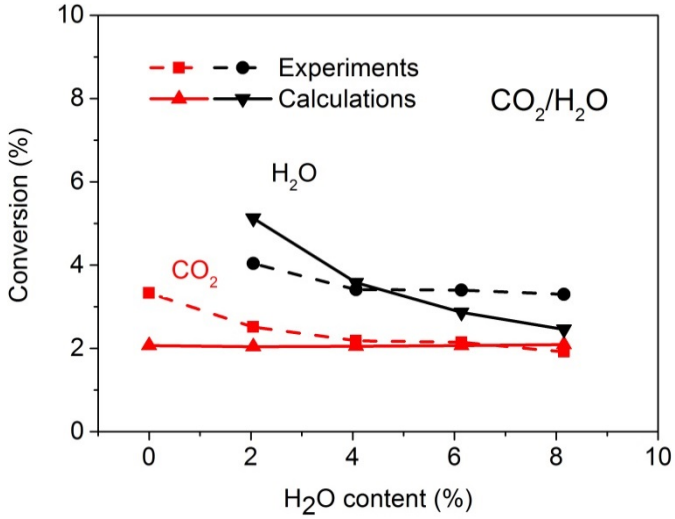

Figure 4. Comparison of the calculated absolute conversion of CO_2 and H_2O, as obtained from our new comprehensive plasma chemistry model, with measured data adopted from ref. (73), in a CO_2/H_2O mixture, as a function of water vapor content, for a SEI of 1.1 eV/molecule and a total flow rate of 600 mL/min at 323 K.

2.3 Effect of N_2 as Impurity and Admixture

The modeling studies in the above two sections—and their experimental counterparts—are limited to high purity gases, hence without the presence of impurities. However, in the real world—for which we are trying to design industrial applications—this will never be the case. N_2 will always be an important impurity or even admixture. This must be taken into account in modeling, since it is known that N_2 can influence the plasma physics, and moreover, N_2 has metastable states, which could influence the plasma chemistry. As a result, the next step in plasma chemistry modeling must be the inclusion of these real world impurities into existing models.

2.3.1 Effect of N_2 on CH_4 Reforming

Few modeling studies exist in literature regarding the addition of N_2 to the CH_4 reforming process,[76-81] but to our knowledge, the research group PLASMANT was the only one focusing on both the impurity and admixture level. [81]

The values for the absolute conversion of CH_4, calculated with our new plasma chemistry model, are plotted versus N_2 content in figure 5, showing a good agreement with measured results, obtained in a DBD, for a residence time of 2.2 s and a SEI of 1.5 eV/molecule.[81] Upon addition of N_2, the absolute CH_4 conversion first remains more or less constant or even slightly decreases, and subsequently it increases. This trend results from the interplay of several effects, i.e. the decreasing electron density with increasing N_2 content and the lower reaction rate constants for several three-body reactions with N_2 compared to CH_4 as third body cause a drop in absolute CH_4 conversion, but on the other hand N_2 can also enhance the absolute CH_4 conversion, due to the

dissociation of CH_4 upon collision with N_2 metastable molecules.

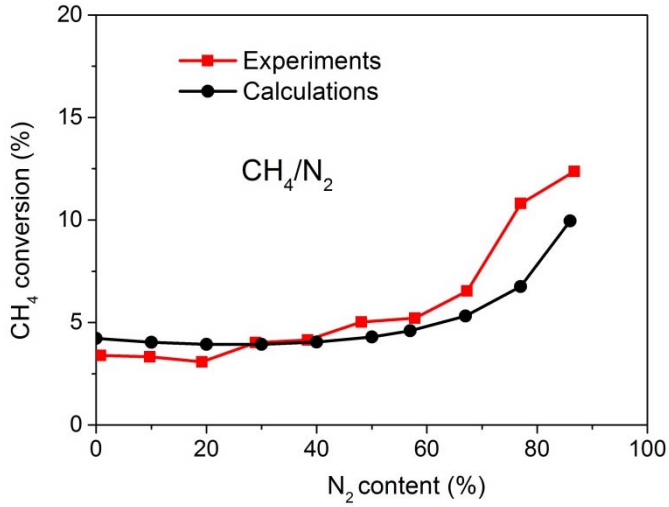

Figure 5. Comparison of the calculated absolute CH_4 conversion, as obtained from our new comprehensive plasma chemistry model, with measured data adopted from ref. (81), in a CH_4/N_2 mixture as a function of N_2 content, for a residence time of 2.2 s and a SEI of 1.5 eV/molecule.

2.3.2 Effect of N_2 on CO_2 Splitting

Investigating the influence of N_2 present during the conversion of CO_2 is of vital importance, since most CO_2 effluent gases contain large fractions of N_2, and the combined presence of N- and O-species is bound to lead to the formation of unwanted NO_x byproducts. The only modeling studies performed here are from the research group PLASMANT. [82-83]

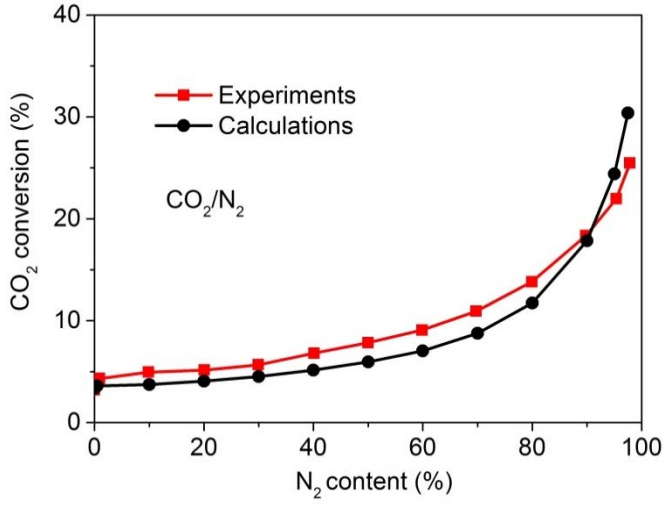

Figure 6. Comparison of the calculated absolute CO_2 conversion, as obtained from our new comprehensive plasma chemistry model, with measured data adopted from ref. (83), in a CO_2/N_2 mixture as a function of N_2 content, for a residence time of 0.73 s and a SEI of 3.0 eV/molecule.

Figure 6 illustrates the absolute CO_2 conversion, calculated with the new plasma chemistry model, in comparison with our previous experimental data, [83] in a CO_2/N_2 mixture as a function of the N_2 content, for a

residence time of 0.73 s and a SEI of 3.0 eV/molecule, showing again a very good agreement. The absolute CO_2 conversion increases more or less exponentially with rising N_2 fraction, both in the experiments and the calculations. This indicates that N_2 has a beneficial effect on CO_2 splitting, due to the dissociation of CO_2 upon collision with N_2 metastable molecules (mainly $N_2(A^3\Sigma_u^+)$).

3. COMPREHENSIVE CHEMICAL KINETICS PLASMA MODEL

It is clear from the previous section that the new plasma chemistry model provides good agreement with our previous (published) experimental data for pure CO_2, as well as binary mixtures (CO_2/CH_4, CO_2/H_2O, CH_4/N_2 and CO_2/N_2), which serves as an important first validation. In this section we will present for the first time the combination of all these chemistry models, and validate it against new experimental data in multi-component mixtures. The temperature-controlled coaxial DBD reactor used for these new experiments has been introduced in previous work. [84-85] This new comprehensive chemistry model can be used to investigate any desired multi-component mixture, containing CO_2, CH_4, N_2, O_2 and H_2O in its feed. We will start by giving a brief explanation of the model, as well as an overview of the included plasma chemistry and how it was developed. Subsequently we will look into the results of some multi-component mixtures, i.e. $CO_2/CH_4/N_2$; $CO_2/CH_4/N_2/O_2$; and $CO_2/CH_4/N_2/H_2O$. For these mixtures we will compare the calculated and measured conversions of CO_2 and CH_4, and the product selectivities, at various gas mixing ratios, for the purpose of validation. Indeed, the present (experimental) results were not optimized; they were only obtained at a fixed condition of flow rate and power, so not focusing on the highest conversion or product selectivities, but they only serve to validate the new chemical kinetics model. Finally, we will discuss in detail the underlying chemistry as predicted by the model, in order to explain the observed trends in conversion and product selectivities.

3.1 Plasma Chemistry Model

There exist different types of models for non-LTE plasmas, [86-88] but the most straightforward approach to model a detailed plasma chemistry is a 0D chemical kinetics model, also called global model. It is based on solving balance equations for the densities of the various plasma species (i.e., various types of molecules, radicals, atoms, ions, excited species, and the electrons), based on production and loss terms, as defined by chemical reactions. [15-16] Details of the model that is used here to describe the plasma chemistry of CO_2 and CH_4 conversion in the multi-component mixtures are presented in the Supporting Information.

As indicated in section 2, within the PLASMANT group several different plasma chemistry models have been developed in the past 5 to 10 years, not only for gas conversion applications, but also for other reactive gas mixtures. The most important chemistries used here for developing our new comprehensive plasma chemistry model for a DBD plasma, are (i) the pure CO_2 chemistry model of Aerts et al.[29,33]; (ii) a model containing the H_2O/O_2 chemistry by van Gaens et al. [89]; (iii) the interaction of CO_2 and CH_4 in the DRM process developed by De Bie et al.[65] and Snoeckx et al.[63]; (iv) a chemistry set describing the interaction between CO_2 and H_2O in the work of Snoeckx et al.[73]; (v) a model containing the CH_4/N_2 chemistry by Snoeckx et al.[81]; and finally (vi) chemistry models describing the interaction in CO_2/N_2 plasmas by Heijkers et al.[82] and Snoeckx et al.[83]. All these different chemistry models were developed and used to investigate specific problems in

combination with experiments for pure CO_2 splitting, in humid air, for dry reforming of methane, artificial photosynthesis, and the influence of N_2 on CH_4 reforming and on pure CO_2 splitting, respectively. In this section we combine all this knowledge from previous research on the different single component, two component and impurity mixtures, to arrive at a new comprehensive chemistry model, which can be used to investigate any desired multi-component mixture containing CO_2, CH_4, N_2, O_2 and H_2O in its feed. To achieve this, the chemistry from the above mentioned models was adopted, adapted and expanded with additional reactions. This led to a model containing 137 species as listed in Table 1. Note that the model does not include vibrationally excited molecules, in contrast to other models developed within PLASMANT. [30-38,82] Indeed, the plasma chemistry model presented here is applied to a DBD plasma (see Section 2 and Figure 1), where vibrationally excited species are of minor importance. [33, 35] In microwave (MW) or gliding arc (GA) discharges, however, vibrationally excited species are very important, [30-32,34-38,82] and thus, the model would have to be extended to these species, to account for their role in the conversion mechanisms (see Conclusions and Outlook).

These 137 species react with each other through 355 electron impact reactions, 631 ion reactions, and 743 neutral reactions. The full list of all these reactions can be found in the Supporting Information, together with their corresponding rate coefficients and the references where these data were adopted from. The model itself is based on solving balance equations for all species densities, with production and loss terms defined by chemical reactions, as explained in the Supporting Information. In addition, a Boltzmann equation is used to calculate the rate coefficients of all the electron impact reactions. The processes included in this Boltzmann equation are elastic collisions, electron impact vibrational excitation/de-excitation, electronic excitation/de-excitation (both dissociative and non-dissociative), electron attachment, as well as electron impact ionization of various important species (see table S1 in the Supporting Information).

As validation of this newly developed chemistry set, we compared the calculated conversions with measured values for different gas mixtures obtained from our earlier work; see figures 2-6 above. These simulations were performed for exactly the same operating conditions as in the experiments. Furthermore, additional experiments were performed for the new multi-component mixture containing CO_2, CH_4, N_2, O_2 and H_2O, for extra validation of the new model, which will be presented below. For more details of the model and the additional experiments, as well as the definitions of gas conversion and product selectivities, we refer to the Supporting Information.

Table 1. Overview of the species included in the model

Molecules	Charged species	Radicals	Excited species
C_3H_8, C_3H_6, C_2H_6, C_2H_4, C_2H_2, CH_4	$C_2H_6^+$, $C_2H_5^+$,$C_2H_4^+$, $C_2H_3^+$, $C_2H_2^+$, C_2H^+, CH_5^+, CH_4^+, CH_3^+, CH_2^+, CH^+	C_4H_2, C_3H_7, C_3H_5, C_2H_5, C_2H_3, C_2H, CH_3, CH_2, CH	
CO_2, CO	CO_2^+, CO^+,CO_3^-, CO_4^-, CO_4^+,$C_2O_4^+$, $C_2O_3^+$, $C_2O_2^+$	C_2O	$CO_2(E1)$, $CO_2(E2)$
C_2N_2		CN, NCN	
H_2O, H_2O_2	H_2O^+, H_3O^+, OH^+, OH^-	HO_2, OH	
N_2H_4, NH_3, N_2H_2	NH_4^+, NH_3^+, NH_2^+, NH^+	NH_2, NH, N_2H,	

		N_2H_3	
N_2O, N_2O_3, N_2O_4, N_2O_5	NO^+, N_2O^+, NO_2^+, NO^-, N_2O^-, NO_2^-, NO_3^-, $O_2^+N_2$	NO, NO_2, NO_3	
CH_2CO, CH_3OH, CH_3CHO, CH_3OOH, C_2H_5OH, C_2H_5OOH, CH_2O		CHO, CH_2OH, CH_3O, CH_3O_2, C_2HO, CH_3CO, CH_2CHO, C_2H_5O, $C_2H_5O_2$	
HCN		H_2CN	
		ONCN,NCO	
	C_2^+, C^+	C, C_2	
N_2	N_2^+, N^+, N_3^+, N_4^+	N	$N_2(a'\Sigma_u^-)$, $N_2(C^3\Pi_u)$, $N_2(V)$, $N_2(A^3\Sigma_u^+)$, $N_2(B^3\Pi_g)$ N(2P), N(2D)
H_2	H_2^+, H^+, H^-, H_3^+,	H	H(2P), $H_2(V)$, $H_2(E)$
O_3, O_2	O_3^-, O_4^-, O_4^+, O_2^-, O_2^+, O^+, O^-	O	O(1D), O(1S), $O_2(a1)$,$O_2(b1)$
	e^-		

3.2 Plasma Conversion and Product Selectivity

3.2.1 $CO_2/CH_4/N_2$ Mixture: Varying CO_2 and N_2 Content

Effluent gas flows from industrial and Carbon Capture Sequestration/Utilization/Recycling (CCS/U/R) often contain impurities, of which in most cases N_2 is the main component. Therefore, it is of interest to study the CO_2 and CH_4 conversion in the presence of N_2. Figure 7 shows the measured and calculated absolute CO_2 and CH_4 conversions (a) and the product selectivities (b) plotted as a function of the CO_2 (and N_2) content in a $CO_2/CH_4/N_2$ mixture, keeping the CH_4 content fixed at 10 %.

At all the gas mixing ratios investigated, the CH_4 conversion is much higher than the CO_2 conversion. This can be explained because the rate of electron impact dissociation of CH_4 is higher than that of CO_2, due to the lower C-H bond dissociation energy. Although there is some small deviation in the exact trend with increasing CO_2 content, in general the calculated values show reasonable agreement with the experiments.

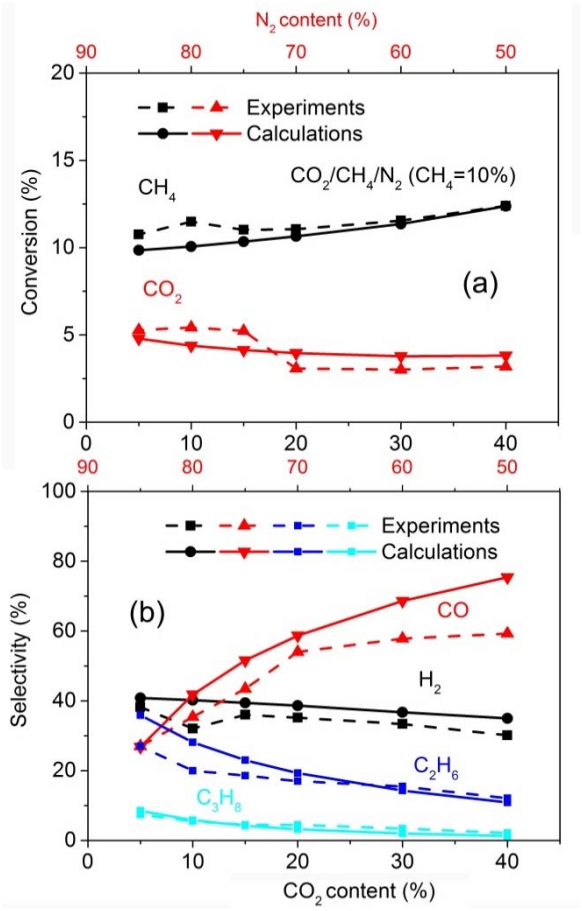

Figure 7. Comparison of the calculated and measured conversion of CH_4 and CO_2 (a), and selectivities of the most important products (b), in a $CO_2/CH_4/N_2$ mixture, as a function of the CO_2 (and N_2) content, for a fixed total flow rate of 200 ml/min and plasma power of 10 W, corresponding to an SEI of 0.76 eV/molecule. The CH_4 content was fixed at 10 %, with the remainder being CO_2 and N_2.

The CO_2/CH_4 ratio has an important influence on the product selectivities, as is clear from figure 7(b). At low CO_2/CH_4 ratio (CO_2 content of 5%), the selectivities of the hydrocarbons (mainly C_2H_6) are comparable or even slightly higher than that of CO. With increasing CO_2/CH_4 ratio, the selectivities of the hydrocarbons and H_2 steadily decrease, while the CO selectivity increases, which is logical as CO is the major product of CO_2 splitting, while the hydrocarbons and H_2 originate from CH_4 dissociation. Increasing the CO_2/CH_4 ratio from 0.5 to 4 yields a drop in the H_2/CO ratio from 2.45 to 0.42. These results show that the H_2/CO ratio can be varied in a wide range, simply controlled by the inlet gas mixing ratio. This is an advantage compared to classical processes, including steam reforming, partial oxidation, and CO_2 reforming, which typically produce syngas with H_2/CO molar ratios of >3, <2, and <1, respectively. [90-91] Finally, we conclude from figure 7(b) that the calculated selectivities are in good agreement with the experiments.

3.2.2 $CO_2/CH_4/N_2$ Mixture: Varying N_2 Content

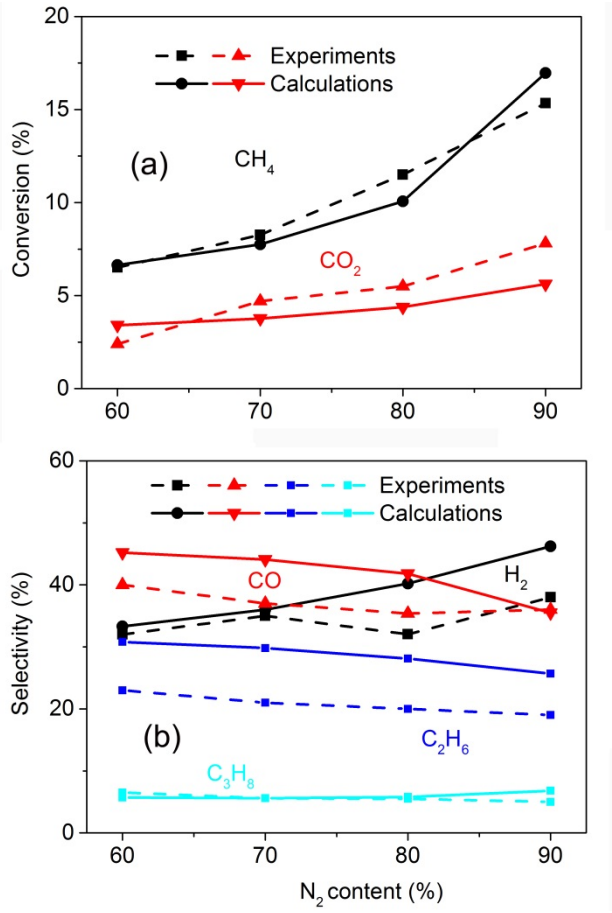

Figure 8. Comparison of the calculated and measured conversion of CH_4 and CO_2 (a), and selectivities of the most important products (b), in a $CO_2/CH_4/N_2$ mixture, as a function of the N_2 content, for a fixed 1:1 CO_2/CH_4 ratio, a fixed total flow rate of 200 ml/min and a corresponding SEI of 0.76 eV/molecule.

Figure 8 illustrate the effect of N_2 content on the experimental and calculated absolute CO_2 and CH_4 conversions (a) as well as on the product selectivities (b) keeping the CO_2/CH_4 ratio fixed at 1. Again good agreement is reached between calculated and measured results, especially for the conversions. Figure 8(a) shows that increasing the N_2 content leads to a higher absolute conversion for both CO_2 and CH_4, both in the experimental and simulation results. This is mainly caused by the increasing role of the N_2 metastable states in the dissociation of both CO_2 and CH_4, as will be discussed in more detail in section 3.3.

In our previous work, we investigated the effect of N_2 for both pure CH_4 [81] and pure CO_2 splitting [83] and in both cases the presence of N_2 led to unwanted effects, i.e. soot deposition and NO_x production, respectively. However, when combining both gases into the current $CO_2/CH_4/N_2$ mixture, no excessive soot deposition or NO_x production is observed. This can be explained by the chemical kinetics model. Indeed, the O-species, which react with N-species to form NO_x in the CO_2/N_2 mixture, form H_2O in the presence of a hydrogen source due to the faster rates of the latter reactions. Vice versa, the O-species prevent the occurrence of soot deposition by oxidation of the carbon containing species.

The major products in this $CO_2/CH_4/N_2$ mixture are again CO, H_2, C_2H_6 and C_3H_8. The measured and calculated selectivities show only a weak dependence on the N_2 content within the investigated range, except

for the calculated H_2 selectivity, which clearly rises upon rising N_2 content, while the measured values show only a very weak increase. The calculated CO, H_2 and C_2H_6 selectivities are somewhat higher than the experimental data, which might be attributed to the limitation of the 0D model, neglecting transport and surface reactions. The latter may become important in some conditions. In contrast, excellent agreement between calculations and experiments is reached for the C_3H_8 selectivity. In general, we consider the agreement between calculated and measured selectivities as fairly good, in view of the complex chemistry and the limitations of the 0D model.

It is worth to mention that, although the CO_2/CH_4 ratio is kept constant, the experimental and calculated syngas (H_2/CO) ratio slightly rises upon increasing N_2 content, i.e. from 1.16 to 1.40 in the experiments and from 0.97 to 1.96 in the calculated values, as can be deduced from the rising H_2 selectivities and the decreasing CO selectivities in figure 8 (b). The reason for the latter will be explained in section 3.3 below.

3.2.3 $CO_2/CH_4/N_2/O_2$ Mixture: Varying O_2 (and N_2) Content

In literature, POX is widely used because O_2 is very effective for low-temperature plasma activation of methane. However, a possible drawback of POX is an excessive oxidation, resulting in the formation of CO_2. The use of CO_2 as a milder oxidant with a little addition of O_2 may combine the advantages of DRM and POX and have a positive influence on the products formed. Therefore, we also investigate the influence of O_2 addition on the CO_2 and CH_4 conversions, as well as on the product selectivities, as presented in figures 9 (a) and 9 (b), respectively.

The addition of O_2 leads to a higher CH_4 conversion while the CO_2 conversion decreases. Indeed, POX becomes the dominant process over DRM. As a result, part of the converted CH_4 is oxidized towards CO and CO_2, which explains the lower CO_2 conversion. The calculated CH_4 conversion is in good agreement with experiments, but there is some discrepancy for the CO_2 and O_2 conversion. This might be attributed to the occurrence of carbon deposition on the surface of the DBD reactor, which will be oxidized to CO and CO_2 by O-species. Since the model does not take surface reactions into account, this process is neglected, which could explain the somewhat higher CO_2 conversion in the model than in the experiments. Furthermore, this may also explain the deviation in the calculated and measured O_2 conversion and the underestimated CO selectivity (see figure 9 (b). However, we consider the agreement still as satisfactory, in view of the complex chemistry and limitations of the model.

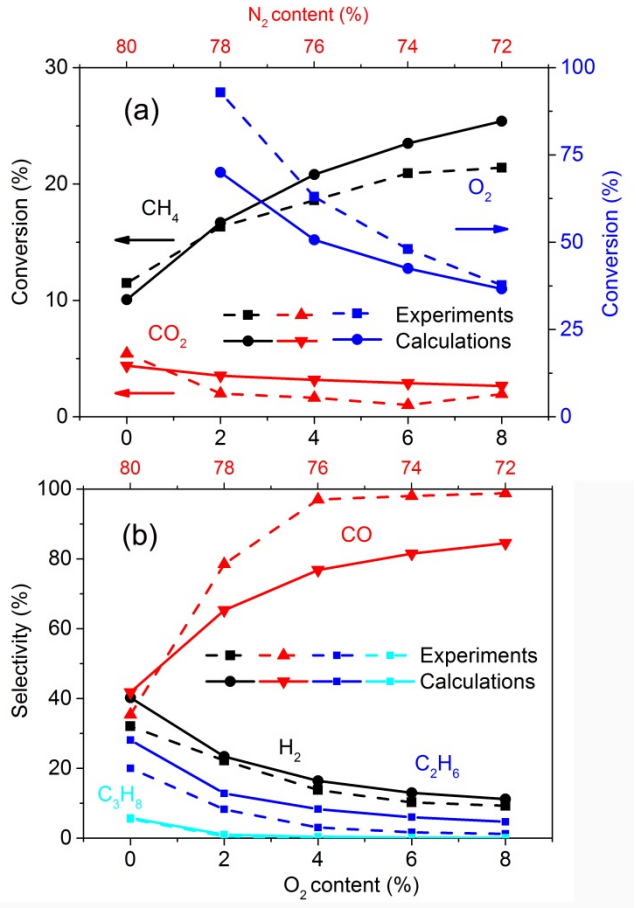

Figure 9. Comparison of the calculated and measured conversions of CH_4, CO_2 and O_2 (a), and selectivities of the most important products (b), in a $CO_2/CH_4/N_2/O_2$ mixture, as a function of the O_2 (and N_2) content, for a 1:1 CO_2/CH_4 ratio, a fixed total flow rate of 200 ml/min and a corresponding SEI of 0.76 eV/molecule. The CO_2 and CH_4 content were both 10 %, with the remainder being O_2 and N_2.

Both the experiments and calculations show that the addition of O_2 rapidly decreases the selectivities of the hydrocarbons (mainly C_2H_6 and C_3H_8) and H_2, because of their oxidation into CO and H_2O. Indeed, the CO selectivity rises dramatically for the same reason. This also leads to a significant drop in the syngas ratio upon increasing O_2 content from 0 to 8 %, i.e. from 1.23 to 0.17 in the experiments, and from 1.34 to 0.25 in the calculations. Again, with some exceptions as explained above, quite good agreement is reached between the calculations and experiments.

3.2.4 $CO_2/CH_4/N_2/H_2O$ Mixture: Varying H_2O (and N_2) Content

An interesting co-reactant and hydrogen source for the conversion of CO_2 is H_2O. It is the most ubiquitous and cheapest hydrogen source available, especially compared to CH_4 and H_2. In addition, the combined conversion of CO_2 and H_2O to produce value-added products using renewable energy would successfully mimic the natural photosynthesis process. Our previous study, however, revealed that this process is not an interesting one to pursue by means of plasma technology, due to a severe drop in CO_2 conversion and energy efficiency when adding H_2O. [73] This was mainly attributed to the recombination of CO with OH into CO_2, as well as the recombination of H atoms with O atoms into OH and subsequently H_2O. [73,92]

However, from figure 10 (a), it becomes clear that the combined conversion of CH_4 and CO_2 remains almost unchanged upon addition of H_2O. Hence, the presence of CH_4 seems to counteract the negative effect of H_2O addition, because the H atoms originating from CH_4 dissociation can recombine with the OH radicals, and thus suppress their negative effect, as there will be less OH available for the back reaction from CO to CO_2. Furthermore, the syngas ratio increases (from 1.35 to 1.65 in the experiments, and from 1.34 to 1.50 in the model) upon increasing H_2O content from 0 to 8 %, which means that the added H_2O is successfully converted into H_2 as well, and the formation of H_2O from O and H atoms is limited due to Le Chatelier's principle. [93] Figure 10 (b) shows that the selectivities of both H_2 and CO slightly increase with rising H_2O content, indicating that H_2O addition is beneficial for the production of syngas. Again, in general good agreement is obtained between the experimental and calculated selectivities of the most important products as a function of the H_2O content.

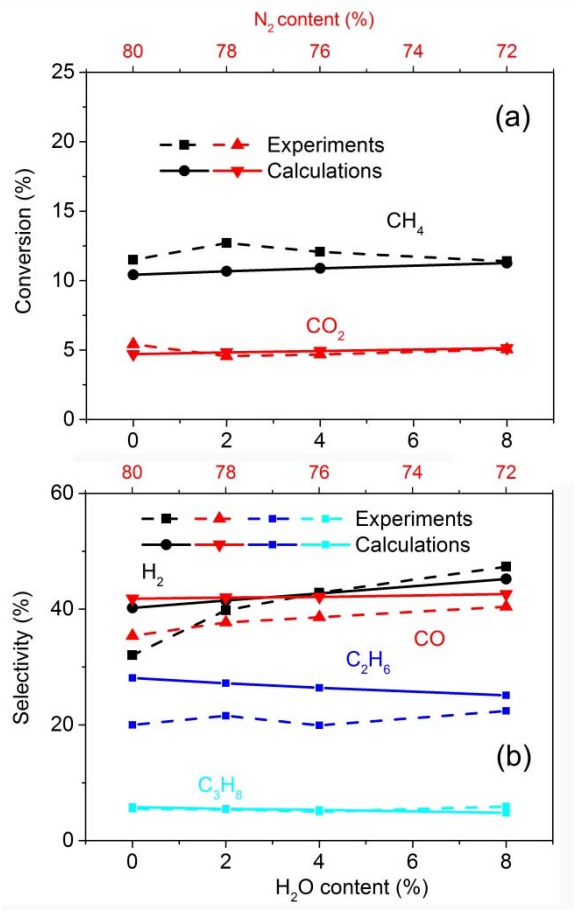

Figure 10. Comparison of the calculated and measured conversion of CH_4 and CO_2 (a), and selectivities of the most important products (b), in a $CO_2/CH_4/N_2/H_2O$ mixture, as a function of the H_2O (and N_2) content, for a 1:1 CO_2/CH_4 ratio, a fixed total flow rate of 200 ml/min and a corresponding SEI of 0.76 eV/molecule. The CO_2 and CH_4 content were both 10 %, with the remainder being H_2O and N_2.

3.3 Underlying Mechanisms of Plasma-based CO_2 and CH_4 Conversion

As the agreement between calculated and measured conversions and product selectivities is quite good, in a wide range of gas mixtures and mixing ratios, we can conclude that our chemical kinetics model can provide

a realistic picture of the plasma chemistry of the DBD reactor for the multi-component mixtures containing CO_2, CH_4, N_2, O_2 and H_2O in its feed. Thus, we can now discuss in more detail the underlying plasma chemistry, as predicted by the model, for both the CO_2 and CH_4 conversion, as well as for the formation of CO, H_2, C_2H_6 and C_3H_8 in the presence of N_2. Similar results, but for the effect of O_2 and H_2O addition, are presented in the SI. This is the most powerful aspect of plasma chemistry modeling. Indeed, a detailed analysis of the reaction pathways allows us to gain a better insight in the underlying chemical reactions and in the overall process. This in turn can help to optimize existing processes, overcome ongoing problems, find new research areas and advance the steps towards a future industrial application of plasma-based gas conversion processes.

3.3.1 CO_2 Conversion

Table 2. Dominant CO_2 loss and formation reactions.

Process	Loss reaction	Process	Formation reaction
L1	$CO_2 + e \rightarrow e + CO + O$	F1	$CO + C_2O_3^+ + M \rightarrow CO_2 + C_2O_2^+ + M$
L2	$CO_2 + N_2(A^3\Sigma_u^+) \rightarrow N_2 + CO + O$	F2	$CO + C_2O_4^+ + M \rightarrow CO_2 + C_2O_3^+ + M$
L3	$CO_2 + N_2(B^3\Pi_g) \rightarrow N_2 + CO + O$	F3	$O + CH_3CO \rightarrow CO_2 + CH_3$
		F4	$CO + OH \rightarrow CO_2 + H$
		F5	$CO_3^- + C_2O_2^+ \rightarrow CO_2 + O + CO + CO$
		F6	$CH_4 + CO_2^+ \rightarrow CO_2 + CH_4^+$
		F7	$CO_3^- + H_3O^+ \rightarrow CO_2 + H_2O + H + O$
		F8	$e + CO_4^+ \rightarrow CO_2 + O_2$
		F9	$CH_2 + O_2 \rightarrow CO_2 + H + H$

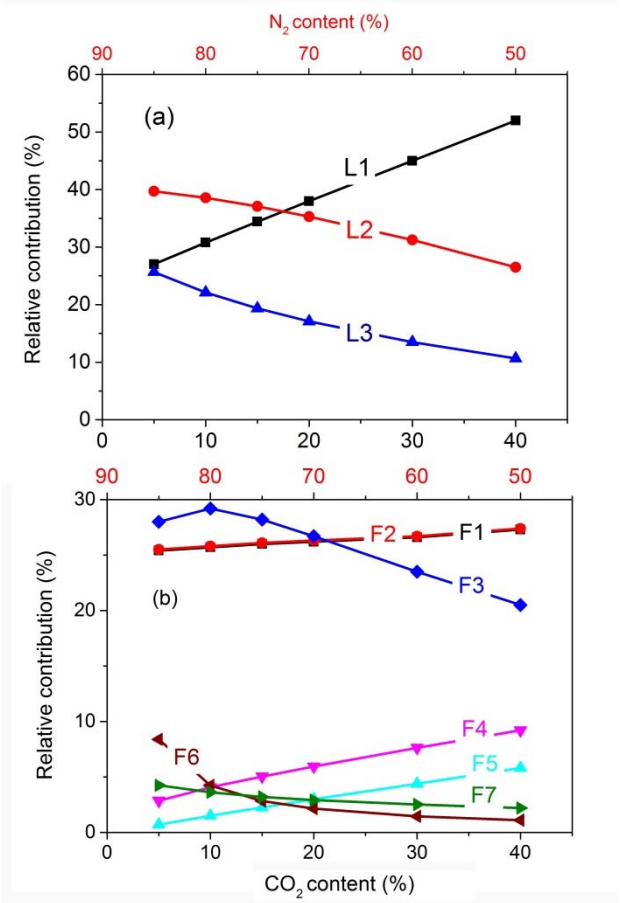

Figure 11. Relative contributions of the main processes leading to CO_2 loss (a) and formation (b) for a $CO_2/CH_4/N_2$ mixture, as a function of the CO_2 (and N_2) content. The total flow rate is fixed at 200 ml/min and the plasma power is 10 W, corresponding to an SEI of 0.76 eV/molecule. The CH_4 content was fixed at 10 %, with the remainder being CO_2 and N_2.

Table 2 lists the most important loss (L1-L3) and formation (F1-F9) processes for CO_2, and figure 11 shows their relative contributions for a $CO_2/CH_4/N_2$ mixture. The CH_4 content was fixed at 10 %, with the remainder being CO_2 and N_2. In the SI, we present similar results for a $CO_2/CH_4/N_2$ mixture at fixed CO_2/CH_4 ratio, as well as upon addition of O_2 or H_2O.

In the absence of O_2 and H_2O (figure 11) and at high CO_2 content (and thus low N_2 content), the most important dissociation reaction of CO_2, at the present DBD conditions, is electron impact dissociation (L1) into CO and O, while at low CO_2 content (and high N_2 content), the dissociation reaction with metastable $N_2(A^3\Sigma_u^+)$ molecules (L2) is dominant, yielding the same splitting products (CO and O). The reaction with metastable $N_2(B^3\Pi_g)$ molecules (L3) also has a non-negligible contribution to the dissociation of CO_2. Upon higher N_2 contents (lower CO_2 contents), the electron energy is gradually being used for N_2 excitation instead of CO_2 dissociation, explaining the drop in the relative contribution of electron impact dissociation and the corresponding increase in the relative contribution of dissociation by N_2 metastable molecules, which provides an alternative dissociation mechanism for CO_2. The same behavior can be seen in the $CO_2/CH_4/N_2$ mixture with fixed (1:1) CO_2/CH_4 ratio (see figure S1 (a) in the SI) and in the presence of O_2 (figure S2 (a)) as well as in the presence of H_2O (figure S3 (a) in the SI). Thus, at high N_2 content, the major loss process of CO_2 is due to N_2

metastable states (reactions L2 and L3) and this explains why the presence of N_2 enhances the CO_2 conversion (See figure 8 in section 3.2.2).

If we take a look at the CO_2 formation in the $CO_2/CH_4/N_2$ mixture, the most significant processes are the ones between CO and the positive ions $C_2O_3^+$ and $C_2O_4^+$, through three-body reactions (F1, F2) as well as the neutral reactions between O atoms and CH_3CO molecules (F3); see figure 11 (b) as well as figure S1 (b) in the SI. A similar conclusion can be obtained for the addition of H_2O (figure S3 (b) in the SI).

With the addition of O_2, the behavior is a bit different. Indeed, the $CO_2/CH_4/O_2$ mixture gives rise to a high concentration of OH radicals. As a result, the reaction between CO and OH, leading to CO_2 and H atoms, becomes the dominant CO_2 formation process at O_2 contents above 5 % (see figure S2 (b): F4). This explains why the addition of O_2 leads to a decrease in CO_2 conversion as indicated in figure 9 in section 3.2.3. This was also the case in our previous study for a CO_2/H_2O mixture, and resulted in a drop in CO_2 conversion upon H_2O addition. [73] In the $CO_2/CH_4/N_2/H_2O$ mixture, however, the addition of H_2O does not cause a drop in absolute CO_2 conversion, as presented in figure 10 above, because the presence of CH_4, and thus H atoms, counteracts the negative effect of the OH radicals, as explained in section 3.2.4 above.

Besides the recombination between CO and OH (F4), electron recombination with CO_4^+ (F8) and the reaction between O_2 and CH_2 (F9), which are quasi negligible for CO_2 production in the other gas mixtures, also become important upon addition of O_2 (figure S2 (b)). Other reactions involving ions (F5, F6, and F7) can also contribute to the CO_2 formation, but with a relative contribution no more than 10%.

Finally, it is important to realize that the total formation rate of CO_2 is much smaller (no more than 10%) than the total CO_2 loss rate for a $CO_2/CH_4/N_2$ mixture, as well as a $CO_2/CH_4/N_2/H_2O$ mixture, so the formation processes only have a minor contribution to the net CO_2 conversion at these conditions. However, the addition of O_2 enhances the formation of CO_2. With the addition of 8% O_2, the total CO_2 formation rate reaches 41% of the total CO_2 loss rate.

3.3.2 CH_4 Conversion

Table 3. Dominant CH_4 loss and formation reactions.

Process	Loss reaction	Process	Formation reaction
L1	$CH_4 + e \rightarrow e + CH_3 + H$	F1	$CH_3 + H + M \rightarrow CH_4 + M$
L2	$CH_4 + CH \rightarrow C_2H_4 + H$	F2	$e + C_3H_8 \rightarrow CH_4 + e + C_2H_4$
L3	$CH_4 + N_2(a'\Sigma_u^-) \rightarrow N_2 + C + 2H_2$	F3	$CH_5^+ + H_2O \rightarrow CH_4 + H_3O^+$
L4	$CH_4 + N_2(A^3\Sigma_u^+) \rightarrow N_2 + CH_3 + H$		
L5	$CH_4 + N_2(a'\Sigma_u^-) \rightarrow N_2 + CH_3 + H$		
L6	$CH_4 + N_2(a'\Sigma_u^-) \rightarrow N_2 + CH_2 + H_2$		
L7	$CH_4 + O \rightarrow CH_3 + OH$		

L8	$CH_4 + OH \rightarrow CH_3 + H_2O$		

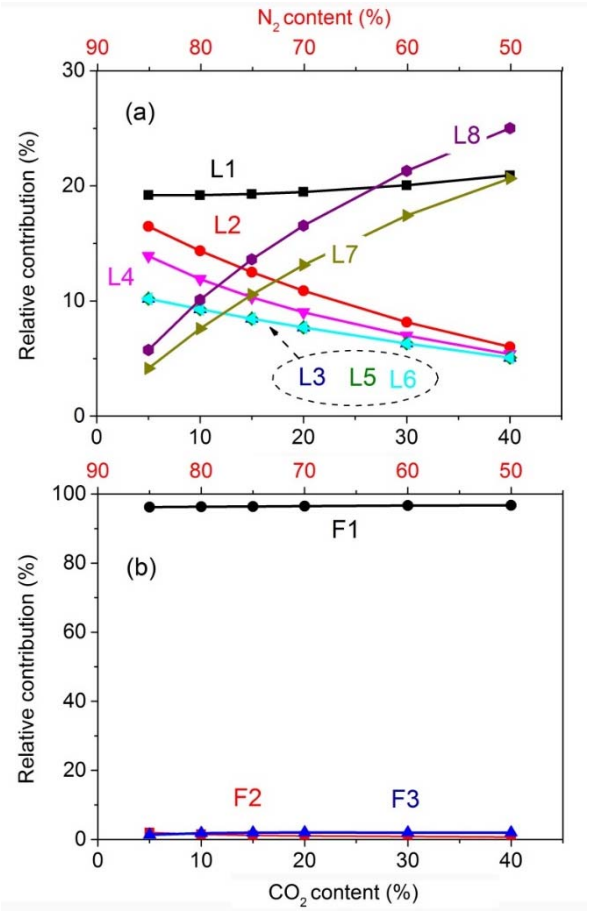

Figure 12. Relative contributions of the main processes leading to CH_4 loss (a) and formation (b) for a $CO_2/CH_4/N_2$ mixture, as a function of the CO_2 (and N_2) content. The total flow rate is fixed at 200 ml/min and the plasma power is 10 W, corresponding to an SEI of 0.76 eV/molecule. The CH_4 content was fixed at 10 %, with the remainder being CO_2 and N_2.

Table 3 lists the most important loss (L1-L8) and formation (F1-F3) processes for CH_4 and in figure 12 the relative contributions of these processes are plotted as a function of CO_2 (and N_2) content in the $CO_2/CH_4/N_2$ mixture, at fixed CH_4 content of 10 %, with the remainder being CO_2 and N_2. The results in the $CO_2/CH_4/N_2$ mixture with fixed CO_2/CH_4 ratio, as well as upon addition of O_2 or H_2O, are presented in figures S4-S6 of the SI.

It is clear from figure 12 that the dominant loss reactions change with increasing CO_2 content (N_2 content). Electron impact dissociation of CH_4 (L1) is always an important loss process at the present DBD conditions. It shows little dependence on the CO_2 content in figure 12. The reaction between CH and CH_4 leading to C_2H_4 and H (L2) is also relatively important for CH_4 dissociation at low CO_2 content. The same applies for the reactions with N_2 metastable singlet and triplet states (reactions L3-L6, and especially L4).

Figure 12 shows that the dissociation process of CH_4 by metastable nitrogen molecules (L3+L4+L5+L6)

could be more important than the direct electron impact processes (L1). The rate coefficients of these processes are subject to some uncertainties, and this will affect the exact values of the relative contributions of these processes, predicted by the model. Nevertheless, we expect the general trends to be valid. Indeed, similar conclusions were made in literature, [81] using the same reaction rate coefficients as in our work for the reactions with N_2 metastable singlet and triplet states (reactions L3-L6), and good agreement was reached with experiments, regardless of the conditions.

With increasing CO_2 content, the reactions between CH_4 and O atoms or OH radicals (L7 and L8) become increasingly important, and their relative contribution towards CH_4 loss even exceeds the contribution of electron impact dissociation (L1) at the highest CO_2 contents (and lowest N_2 contents) investigated. It should be noted that electron impact vibrational excitation of CH_4 is also important as loss process for the CH_4 ground state molecules, but this process is only taken into account in our model as energy loss for the electrons, and not as a chemical loss process for CH_4, because the vibrationally excited species are not considered separately in our model. Indeed, electron impact vibrational excitation mainly takes place in the lower electron energy range, and thus it is of lower importance when the reduced electric field (i.e., ratio of electric field over gas density) is quite high, such as in a DBD plasma.[33]

In the $CO_2/CH_4/N_2$ mixture with fixed 1:1 CO_2/CH_4 ratio, a similar behavior is observed (see figure S4 (a) in the SI), except that the relative contribution of electron impact dissociation clearly drops upon increasing N_2 content, because of the drop in CH_4 content. With high N_2 content, the dissociation of CH_4 due to collisions with N_2 metastable states (reactions L3–L6) becomes most important, explaining why the presence of N_2 enhances the CH_4 conversion (see figure 8 in section 3.2.2).

Upon addition of O_2 to the mixture, the loss reaction of CH_4 with OH radicals (L8) is dominant (figure S5 (a) in SI). Its relative contribution gradually increases with higher O_2 contents, because the concentration of produced OH radicals rises during both the microdischarge filaments and afterglow stages of the DBD. The same applies, to a lower extent, for the loss reaction upon collision with O atoms (L7). This explains why the CH_4 conversion rises drastically upon increasing O_2 content (see figure 9 in section 3.2.3).

H_2O addition has no significant effect on the relative contributions of the various loss processes, except that the reaction with N_2 metastable triplet states $N_2(A^3\Sigma_u^+)$ (L4) drops and the reaction with OH radicals (L8) rises (see figure S6 (a) in the SI), due to a decreasing concentration of $N_2(A^3\Sigma_u^+)$ and increasing concentration of OH radicals, respectively.

If we take a look at the formation processes, the three-body recombination of CH_3 radicals with H atoms (F1) is the dominant formation process at all the investigated conditions (see figure 12 (b), as well as figures S4 (b), S5 (b) and S6 (b) in the SI). Other reactions, such as electron impact dissociation of C_3H_8 into CH_4 (F2) and charge transfer between H_2O and CH_5^+ (F3), have relative contributions of less than 5% to the CH_4 formation.

If we compare the total formation rate with the total loss rate of CH_4, we can conclude that the total formation rate is relatively large (up to 40%) compared to the total CH_4 loss rate, at least without O_2 addition. Hence, this behavior is different from the CO_2 loss and formation rates, as mentioned above. The reason is that

the three-body recombination of CH_3 radicals with H atoms is very important outside the microdischarge filaments in the DBD reactor (see SI for more details on how the microdischarge filaments in the DBD are treated: they are treated as afterglow in between discharge pulses). A similar behavior was reported by Snoeckx et al.[63] However, upon O_2 addition, the formation processes have a decreasing contribution to the net CH_4 conversion (formation rate no more than 10% of the total CH_4 loss rate with 8% O_2 addition), explaining again why the CH_4 conversion drastically rises upon O_2 addition (see figure 9).

3.3.3 CO Production

Table 4. Dominant CO formation and loss reactions.

Process	Formation reaction	Process	Loss reaction
F1	$e + CO_2 \rightarrow CO + e + O$	L1	$CO + C_2O_3^+ + M \rightarrow C_2O_2^+ + CO_2 + M$
F2	$N_2(A^3\Sigma_u^+) + CO_2 \rightarrow CO + N_2 + O$	L2	$CO + C_2O_4^+ + M \rightarrow C_2O_3^+ + CO_2 + M$
F3	$CH_2O + O \rightarrow CO + OH + H$	L3	$CO + N \rightarrow CN + O$
F4	$N_2(B^3\Pi_g) + CO_2 \rightarrow CO + N_2 + O$	L4	$CO + CH + N_2 \rightarrow C_2HO + N_2$
F5	$H + CHO \rightarrow CO + H_2$	L5	$CO + H + M \rightarrow CHO + M$
		L6	$CO + OH \rightarrow CO_2 + H$
		L7	$CO + O(1D) \rightarrow CO_2$

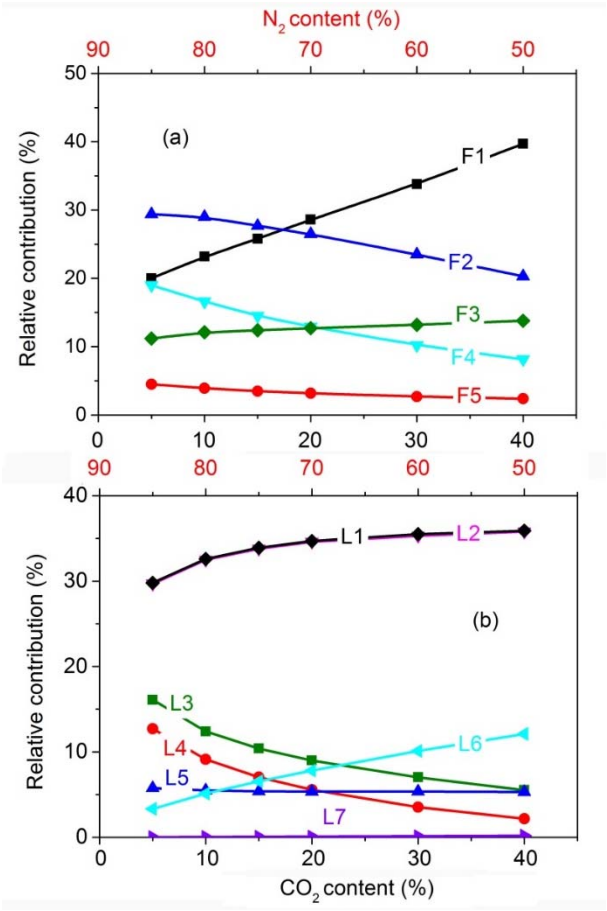

Figure 13. Relative contributions of the main processes leading to CO formation (a) and loss (b) for a $CO_2/CH_4/N_2$ mixture, as a function of the CO_2 (and N_2) content. The total flow rate is fixed at 200 ml/min and the plasma power is 10 W, corresponding to an SEI of 0.76 eV/molecule. The CH_4 content was fixed at 10 %, with the remainder being CO_2 and N_2.

As CO is the major product of the CO_2 conversion, with a selectivity of about 30–100 % (see figures 7-10 above), we present here the dominant reaction pathways for the formation and loss of CO, to obtain a better understanding of the influence of the CO_2/CH_4 ratio, the N_2 content, and the addition of O_2 or H_2O on the CO yield. Table 4 lists the most important formation (F1-F5) and loss (L1-L7) processes for CO. Their relative contributions in the $CO_2/CH_4/N_2$ mixture are plotted in figure 13, as a function of the CO_2 (and N_2) content. The corresponding results at fixed CO_2/CH_4 ratio, as well as upon addition of O_2 or H_2O, are presented in figures S7-S9 of the SI.

Electron impact dissociation of CO_2 (F1), as well as dissociation of CO_2 upon collision with N_2 metastable singlet and triplet states (F2 and F4), are the dominant formation processes of CO, at all conditions investigated (see figure 13 (a), and figures S7 (a) and S9 (a) in the SI), except upon addition of O_2. Furthermore, the reaction between CH_2O and O, leading to CO, OH and H (F3), also plays a quite important role, and this process even becomes the prime source of CO when O_2 is added (see figure S8 (a) in the SI). This additional channel for CO production explains why the addition of O_2 leads to a drastic increase in CO selectivity (see figure 9).

As far as the loss of CO is concerned, the three-body reactions between CO and the positive ions $C_2O_3^+$

and $C_2O_4^+$ (L1, L2) are dominant at all conditions (see figure 13 (b), and figures S7 (b) and S9 (b) in the SI), except upon addition of O_2. These two reactions are also the most important for CO_2 formation (see section 3.3.1 above). Upon addition of O_2, however, the reaction of CO with OH becomes the most important route towards CO loss (L6, in figure S8 (b)), which is also the dominant process of CO_2 formation under these conditions.

Besides the CO loss reactions towards CO_2 formation (L1, L2, L6, L7), other loss channels include the reaction of CO with N, leading to CN and O (L3), the reaction with CH, leading to C_2HO (L4), and the reaction with H, producing CHO (L5), which have relative contributions up to 20 % at the conditions investigated.

Finally, it is important to realize that the total loss rate of CO is much smaller (no more than 6 %) than the total CO formation rate for all gas mixtures and mixing ratios investigated, so the loss processes only have a minor contribution to the net CO formation at these conditions.

3.3.4 H_2 Production

Table 5. Dominant H_2 formation and loss reactions.

Process	Formation reaction	Process	Loss reaction
F1	$N_2(a'\Sigma_u^-) + CH_4 \rightarrow 2H_2 + N_2 + C$	L1	$H_2 + C \rightarrow CH + H$
F2	$H_2CN + H \rightarrow H_2 + HCN$	L2	$H_2 + OH \rightarrow H_2O + H$
F3	$N_2(a'\Sigma_u^-) + CH_4 \rightarrow H_2 + N_2 + CH_2$	L3	$H_2 + e \rightarrow e + H + H$
F4	$e + C_2H_6 \rightarrow H_2 + e + C_2H_4$	L4	$H_2 + O \rightarrow OH + H$
F5	$CH_2 + H \rightarrow H_2 + CH$	L5	$H_2 + N(2P) \rightarrow NH + H$
F6	$CH_3OH + H \rightarrow H_2 + CH_2OH$		
F7	$CHO + H \rightarrow H_2 + CO$		
F8	$CH_3OH + H \rightarrow H_2 + CH_3O$		
F9	$CH_3 + O \rightarrow H_2 + CO + H$		

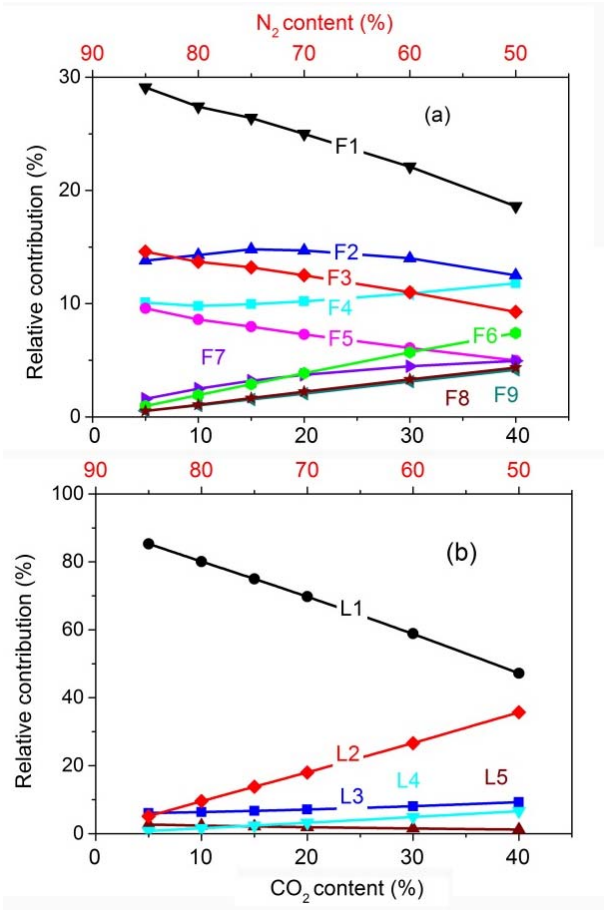

Figure 14. Relative contributions of the main processes leading to H_2 formation (a) and loss (b) for a $CO_2/CH_4/N_2$ mixture, as a function of the CO_2 (and N_2) content. The total flow rate is fixed at 200 ml/min and the plasma power is 10 W, corresponding to an SEI of 0.76 eV/molecule. The CH_4 content was fixed at 10 %, with the remainder being CO_2 and N_2.

H_2 is also a significant product, due to the CH_4 conversion, with a selectivity of about 10–50 % (see figures 7-10 above). Table 5 lists the most important formation (F1-F9) and loss (L1-L5) processes for H_2 and figure 14 illustrates the relative contributions of these processes for the $CO_2/CH_4/N_2$ mixture at constant CH_4 content. The results for the other conditions can be found in figures S10 - S12 in the SI.

The most important production process at all conditions investigated is the reaction of CH_4 with $N_2(a'\Sigma_u^-)$ metastable singlet states, producing C atoms and two H_2 molecules (F1). This reaction of course becomes increasingly important with increasing N_2 content. Furthermore, electron impact dissociation of C_2H_6 (F4) is an important formation process at lower N_2 content (see especially figure S10 (a)). The reaction of CH_4 with $N_2(a'\Sigma_u^-)$ towards the production of CH_2 radicals and one H_2 molecule (F3) also contributes to the H_2 production to some extent, as well as the reaction of H_2CN, CH_2 radicals, CHO and CH_3OH with H (reactions F2, F5-F8) and the reaction of CH_3 with O atoms (F9), depending on the conditions.

The dominant loss process is the reaction of H_2 with a C atom producing a CH radical and a H atom (L1) at all gas mixing ratios (see figure 14 (b), and figures S10 (b) and S12 (b) of the SI), except upon addition of O_2 (see figure S11 (b) in the SI). The relative contribution of this reaction, however, rapidly drops with increasing

CO_2 content, because the C atom density decreases due to reaction with O-containing species, such as OH and O_2, which are directly or indirectly formed from CO_2. This also explains why the loss reaction with OH radicals (L2) becomes gradually more important upon rising CO_2 content (see figure 14 (b)). The latter reaction is also dominant upon addition of O_2 (see figure S11 (b) of the SI), for the same reason. The increasing role of reaction L2 in the loss of H_2 also explains why the selectivity of H_2 decreases upon addition of either CO_2 or O_2 (see figures 7 and 9 above). Other reactions, including electron impact dissociation of H_2 (L3), oxidization of H_2 by O atoms generating OH and H (L4), and the reaction of H_2 with excited N atoms towards NH (L5), can also contribute to H_2 loss, but their relative contributions do not exceed 20% at the conditions investigated.

Finally, the total loss rate of H_2 ranges from 13 % to 24 % of the total H_2 formation rate for all gas mixtures and mixing ratios investigated, so the loss processes have a non-negligible contribution to the net H_2 formation at these conditions. Especially O_2 addition enhances the total loss rate of H_2 via reaction L2, as mentioned above.

3.3.5 C_2H_6 Production

Table 6. Dominant C_2H_6 formation and loss reactions.

Process	Formation reaction	Process	Loss reaction
F1	$CH_3 + CH_3 + M \rightarrow C_2H_6 + M$	L1	$C_2H_6 + e \rightarrow e + C_2H_4 + H_2$
F2	$C_2H_5 + H + M \rightarrow C_2H_6 + M$	L2	$C_2H_6 + OH \rightarrow C_2H_5 + H_2O$
F3	$C_2H_5 + CH_3O \rightarrow C_2H_6 + CH_2O$	L3	$C_2H_6 + O \rightarrow C_2H_5 + OH$
F4	$C_2H_5 + CHO \rightarrow C_2H_6 + CO$	L4	$C_2H_6 + N_2(a'\Sigma_u^-) \rightarrow N_2 + C_2H_4 + H_2$
F5	$C_2H_5 + C_2H_5 \rightarrow C_2H_6 + C_2H_4$	L5	$C_2H_6 + N_2(A^3\Sigma_u^+) \rightarrow N_2 + C_2H_4 + H_2$
		L6	$C_2H_6 + e \rightarrow e + C_2H_5 + H$
		L7	$C_2H_6 + CH_2 \rightarrow C_3H_8$

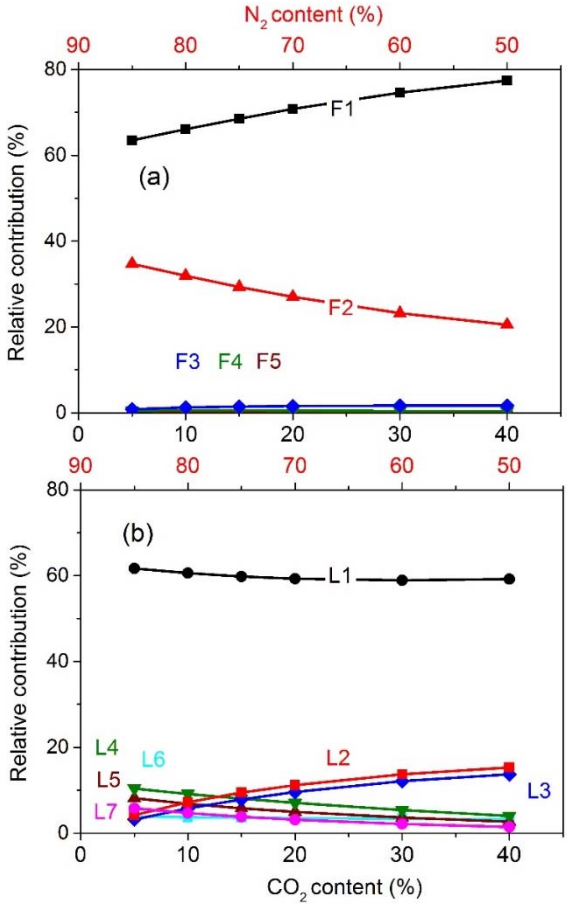

Figure 15. Relative contributions of the main processes leading to C_2H_6 formation (a) and loss (b) for a $CO_2/CH_4/N_2$ mixture, as a function of the CO_2 (and N_2) content. The total flow rate is fixed at 200 ml/min and the plasma power is 10 W, corresponding to an SEI of 0.76 eV/molecule. The CH_4 content was fixed at 10 %, with the remainder being CO_2 and N_2.

Table 6 lists the most important formation (F1-F5) and loss (L1-L7) processes for C_2H_6. In figure 15, the relative contributions of these processes are plotted for a $CO_2/CH_4/N_2$ mixture at fixed CH_4 content. The results at the other conditions are given in figures S13-S15 of the SI.

The dominant formation channel for C_2H_6 in all gas mixtures is three-body recombination of two CH_3 radicals (F1), contributing for more than 60 % to the C_2H_6 formation, and even up to 95 % upon addition of O_2. Upon addition of CO_2 and O_2, the CH_3 radicals are consumed by other competitive channels involving oxygen containing species, and this explains why the C_2H_6 selectivity gradually decreases with the addition of CO_2 and O_2 (see figures 7 and 9). The second most important reaction is three-body recombination of C_2H_5 with H (F2), while the other recombination reactions of C_2H_5 with CH_3O, CHO and C_2H_5 (F3-F5) are of minor importance.

The dominant loss reaction for C_2H_6 at nearly all conditions investigated is electron impact dissociation into C_2H_4 and H_2 (L1). The reaction of C_2H_6 with OH or O towards the production of C_2H_5 (L2-L3) is also relatively important; see especially figure S13 (b) and figure S14 (b). Indeed, upon addition of O_2, L2 even becomes dominant (see figure S14 (b)). Finally, the dissociation of C_2H_6 upon collision with N_2 metastable molecules (both $N_2(a'\Sigma_u^-)$ and $(N_2A^3\Sigma_u^+)$) (L4 and L5) becomes gradually more important upon rising N_2

content, as expected. This explains why the C_2H_6 selectivity slightly decreases upon increasing N_2 content in figure 8.

Finally, the total loss rate of C_2H_6 is 42 to 60 % of the total C_2H_6 formation rate for all gas mixtures and mixing ratios investigated, so the loss processes have a quite large contribution to the net C_2H_6 formation at these conditions. Like for H_2, increasing the O_2 content enhances the total loss rate of C_2H_6.

3.3.6 C_3H_8 Production

Table 7. Dominant C_3H_8 formation and loss reactions.

Process	Formation reaction	Process	Loss reaction
F1	$CH_3 + C_2H_5 + M \rightarrow C_3H_8 + M$	L1	$C_3H_8 + e \rightarrow e + C_3H_6 + H_2$
F2	$C_2H_6 + CH_2 \rightarrow C_3H_8$	L2	$C_3H_8 + e \rightarrow e + C_2H_4 + CH_4$
F3	$C_3H_7 + H \rightarrow C_3H_8$	L3	$C_3H_8 + e \rightarrow e + C_3H_7 + H$

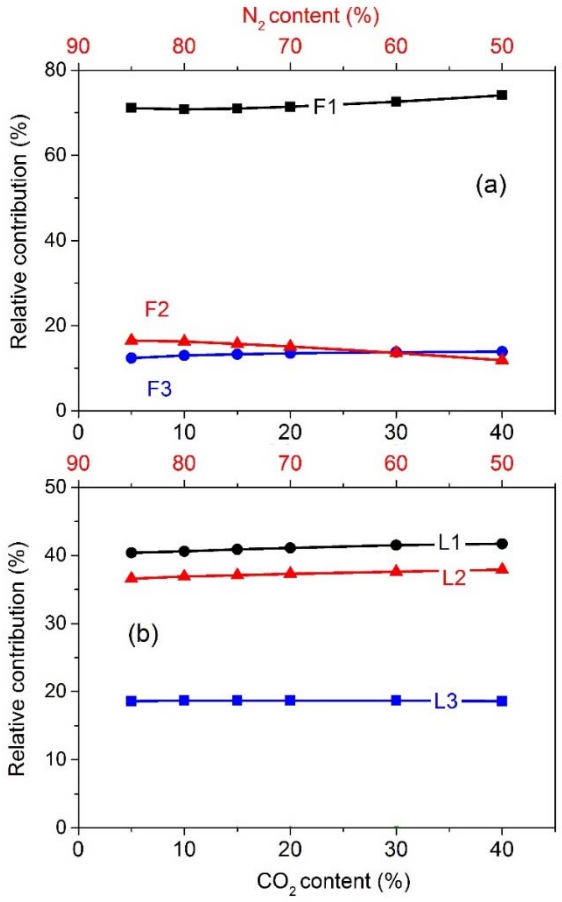

Figure 16. Relative contributions of the main processes leading to C_3H_8 formation (a) and loss (b) as a function of the CO_2 (and N_2) content, for a fixed total flow rate of 200 ml/min and plasma power of 10 W, corresponding to an SEI of 0.76 eV/molecule. The CH_4 content was fixed at 10 %, with the remainder being CO_2 and N_2.

Table 7 lists the most important formation (F1-F3) and loss (L1-L3) processes for C_3H_8, while the relative

contributions of these processes for a $CO_2/CH_4/N_2$ mixture at constant CH_4 content are plotted in figure 16. The results for the other gas mixtures are again presented in the SI (figures S16-S18)

Three-body recombination of C_2H_5 and CH_3 radicals (F1) is the most important formation process. It contributes above 70 % at all conditions investigated, and even up to 90 % upon addition of O_2 (figure S17 (a)). Finally, the loss of C_3H_8 occurs almost entirely through electron impact dissociation (L1-L3 in decreasing order of importance) at all conditions investigated.

Finally, our calculations reveal that the loss of C_3H_8 is quite significant compared to their production, because the total loss rate takes up around 38 to 46% of the total formation rate.

3.3.7 General Overview of the Reaction Pathways

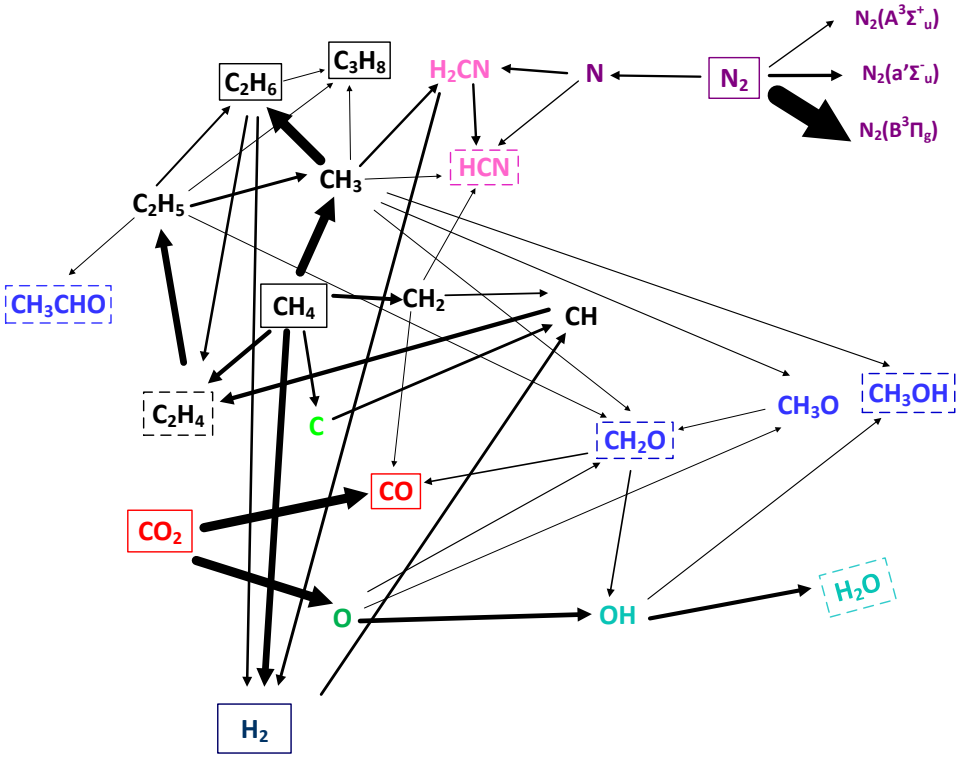

Figure 17. Schematic overview of the dominant reaction pathways for the conversion of CH_4 and CO_2, as well as N_2, in a 1:1:8 $CO_2/CH_4/N_2$ mixture, for a fixed total flow rate of 200 ml/min and plasma power of 10 W, corresponding to an SEI of 0.76 eV/molecule. The thickness of the arrow lines is linearly proportional to the rate of the net reactions. The most important molecules are indicated with a solid line frame, the molecules formed with lower densities are written in a frame with dashed lines, while the radicals are not written in a frame.

From the above detailed analysis of the dominant loss and formation reactions for CH_4, CO_2 and the major products, we can compose a general picture of the dominant reaction pathways in the plasma. This is summarized in figure 17 for a 1:1:8 $CO_2/CH_4/N_2$ mixture, at a fixed total flow rate of 200 ml/min and plasma power of 10 W, corresponding to an SEI of 0.76 eV/molecule.

The conversion process, at the present DBD conditions, starts with electron impact dissociation of CH_4,

forming CH_3 radicals. Meanwhile, electron impact excitation of N_2 produces metastable singlet and triplet states, which also promote the dissociation of CH_4 towards CH_3, CH_2, CH radicals and C atoms. The CH_3 radicals will recombine toward higher hydrocarbons, i.e., mainly C_2H_6 and C_3H_8. Moreover, the recombination between CH_4 and CH produces unsaturated hydrocarbons, i.e. mainly C_2H_4. The latter can recombine with H atoms into C_2H_5 radicals, which further produce other hydrocarbons, such as C_2H_6 and C_3H_8, as well as CH_3 radicals. Furthermore, dissociation of CH_4 and the higher hydrocarbons by electron impact and by collisions with N_2 metastable states yields the formation of H_2.

At the same time, electron impact collisions with N_2 also yield splitting of N_2 into N atoms, which can react with CH_3 radicals to generate H_2CN. The latter are not stable and quickly transform into hydrogen cyanide (HCN) upon impact with N or H atoms. At 80 % N_2 content, our simulation shows that HCN is the most abundant N-containing end product (around 1600 ppm). This indicates that the presence—even in high concentrations—of N_2 does not result in a significant production of N-containing species. This is in qualitative agreement with our experiments, since no N-containing species were detected.

Electron impact dissociation and dissociation upon impact with N_2 metastable states also contribute to the conversion of CO_2 into CO and O. Moreover, the CH_3 radicals, formed by CH_4 dissociation, react with O atoms, to form CH_2O (formaldehyde) and CH_3O radicals. The latter can subsequently be converted into CH_2O as well. Furthermore, the O atoms can react with CH_2O or CH_4 to produce OH radicals, which can further react with CH_3 radicals into CH_3OH (methanol), albeit to a lower extent. The OH radicals also react further into H_2O. Finally, the O atoms, created from CO_2 conversion, initiate the formation of other oxygenates, like acetaldehyde (CH_3CHO). However, this reaction path is not so important, because of the limited formation of O radicals.

In order of decreasing importance, H_2, CO, C_2H_6, H_2O, as well as the hydrogen cyanide (HCN) are the main end products (with molar fractions of 0.80 %, 0.60 %, 0.20 %, 0.19 % and 0.16 %, respectively) in a 1:1:8 $CO_2/CH_4/N_2$ mixture. The fraction of other oxygenates (CH_2O, CH_3OH, etc.) as well as C_3H_8 in the end products is lower than 0.1 %, hence their yields are of minor importance. Note that HCN was not detected in our experiments, although the calculations predict a higher concentration than for C_3H_8. This is because thermal conductivity detectors (TCD) and a flame-ionization detector (FID) were used to detect the products. These detectors are more sensitive and hence have a much lower detection limit for C_3H_8 compared to HCN. Moreover, the yield of water (H_2O) was not calculated in the experiments, since GC measurements are not suitable to deliver quantitative data about H_2O.

Our earlier study showed that the presence of N_2 during CO_2 splitting leads to the formation of N_2O and several NO_x compounds, with concentrations in the range of several 100 ppm. [81] These concentrations are too low to be considered useful for nitrogen fixation [6-7] but will give rise to several environmental problems. N_2O is an even more potent greenhouse gas than CO_2, with a global warming potential (GWP) of 298 CO_2- equivalent, while NO and NO_2 are responsible for acid rain and the formation of ozone and a wide variety of toxic products. However, our calculations predict that with the addition of CH_4, the production of NO_x compounds upon reaction between N- and O-species is prohibited, because of the faster reaction between O- and H-species, as explained in section 3.2 above. Therefore, no NO_x compounds are plotted in figure 17. This result is very

important, as it indicates that DRM in a real gas effluent, containing significant amounts of N_2, would not cause problems of NO_x formation, that are present in CO_2 splitting upon addition of N_2.

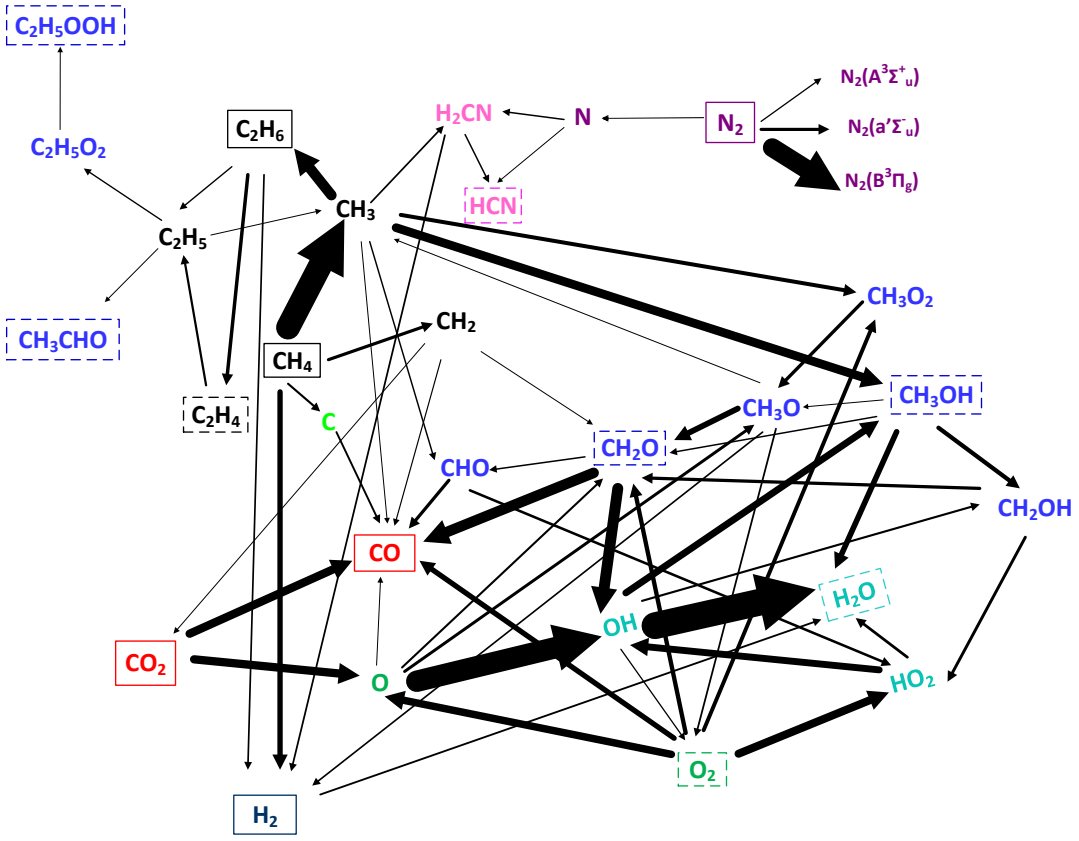

Figure 18. Schematic overview of the dominant reaction pathways for the conversion of CH_4, CO_2, O_2 and N_2 in a 10:10:78:2 $CO_2/CH_4/N_2/O_2$ mixture, for a fixed total flow rate of 200 ml/min and plasma power of 10 W, corresponding to an SEI of 0.76 eV/molecule. The thickness of the arrow lines is linearly proportional to the rate of the net reactions. The most important molecules are indicated with a solid line frame, the molecules formed with lower densities are written in a frame with dashed lines, while the radicals are not written in a frame.

From the analysis of the dominant loss and formation processes in sections 3.3.1-3.3.6 above, it became clear that the addition of water does not change the plasma chemistry to a large extent, because of its limited influence on the CH_4 and CO_2 conversion (see also figure 10 above). Hence, the dominant reaction pathways in a $CO_2/CH_4/N_2/H_2O$ mixture are also well represented by figure 17.

For the $CO_2/CH_4/N_2/O_2$ mixture, on the other hand, the situation is different, because O_2 addition affects the dominant loss and formation reactions, as was clear from sections 3.3.1-3.3.6 above. Therefore, we plot in figure 18 the dominant reaction pathways for the conversion of CH_4, CO_2, O_2 and N_2 in a 10:10:78:2 $CO_2/CH_4/N_2/O_2$ mixture. Again, electron impact dissociation of CH_4 and dissociation upon impact with N_2 metastable singlet and triplet states results in the formation of CH_3 radicals. The latter can again recombine into hydrocarbons, such as ethane (C_2H_6), but the production of higher hydrocarbons through CH_3 recombination is reduced due to the increased recombination rate between CH_3 and O_2 or OH radicals, which are more abundant in case of O_2 addition, yielding methanol (CH_3OH) formation. Moreover, the recombination of CH_3 radicals

and O_2 molecules into CH_3O_2 radicals, which further form CH_3O, also becomes important. The CH_3O radicals also yield the formation of formaldehyde (CH_2O) and methanol (CH_3OH). However, methanol (CH_3OH) can quickly react back into CH_3O radicals through the reverse reactions with O, H or OH radicals at a somewhat larger rate, so our model reveals a net conversion from methanol (CH_3OH) to formaldehyde (CH_2O).

In addition, methanol (CH_3OH) can react further into formaldehyde (CH_2O) through the CH_2OH radicals, and formaldehyde (CH_2O) can further be converted into CO, either directly upon reaction with O atoms or indirectly through the CHO radicals. Furthermore, the reaction of formaldehyde (CH_2O) with O atoms also produces OH radicals. The O_2 molecules are converted into HO_2 radicals, O atoms and CO, as well as formaldehyde (CH_2O). It is worth to mention that most of the O_2 conversion proceeds through collisions between neutral species. For instance, O_2 dissociation upon impact with N_2 metastable states contributes for about 15%, showing the important role of N_2, while electron impact dissociation contributes for only 3-4%.

CO can be further oxidized into CO_2 upon reaction with OH radicals. Furthermore, also the CH_2 radicals can be oxidized into CO_2. These reactions are obviously undesired. The O atoms are also converted into CH_3O and OH radicals, which can again form water. The production of H_2CN upon impact between N and CH_3 radicals is prohibited, due to competition with other reactions that consume CH_3 radicals upon addition of O_2. As a result, the concentration of HCN in the mixture is greatly reduced.

The most important products in a 10:10:78:2 $CO_2/CH_4/N_2/O_2$ mixture, as predicted by our model, are (in order of decreasing importance) H_2O, CO, H_2, ethane (C_2H_6), methanol (CH_3OH) and hydrogen cyanide (HCN), with molar fractions of 1.60 %, 1.30 %, 0.78 %, 0.13 %, 0.10 %, and 0.094 %, respectively. Note that methanol (CH_3OH) was not detected in our experiments, because its concentration approaches the detection limit. In contrast, C_3H_8 species were detected in spite of their lower concentration because of a much lower detection limit.

The comparison of figures 17 and 18 clearly shows that O_2 addition has a dramatic effect on the plasma chemistry of CO_2 and CH_4 conversion, as was also clear from section 3.2 and sections 3.3.1-3.3.6 above (cf. figure 9 and figures S2, S5, S8, S11, S14 and S17 of the SI). A similar behavior was reported by De Bie et al., when comparing the plasma chemistry of DRM (CH_4/CO_2) and POX (CH_4/O_2). Indeed, both investigations indicate that mixtures with CO_2 favor the formation of H_2, while the production of H_2O is greatly promoted upon addition of O_2. CO is formed at high density in both gas mixtures. Note that adding O_2 can effectively promote the conversion of CH_4 (see figure 9). However, also a significant amount of undesired CO_2 is formed and thus the net conversion of CO_2 is greatly reduced. Our pathway analysis shows how plasma chemistry modeling can help to obtain better insight, and this is very valuable to optimize the process. For example, the different pathways revealed by our model can help to determine the most suitable feed gas ratio to obtain the highest yield and/or selectivity of desired products.

4. CONCLUSIONS AND OUTLOOK

Chemical kinetics modeling has proven to be very useful to study the plasma-based conversion of CO_2 and CH_4. In recent years, plasma chemistry models have been developed in a stepwise manner. First models consisted of single component molecular gases, i.e. to study CO_2 splitting and CH_4 reforming. In a next step,

multi-component mixtures were studied, i.e. DRM, POX, artificial photosynthesis, and CO_2 hydrogenation. Subsequently, the effect of N_2 as impurity and admixture on the CO_2 splitting and CH_4 reforming process was investigated, to better approach real effluent gases.

Combining the knowledge gathered in this field so far, we presented here a new comprehensive plasma chemistry set, that can be used for zero-dimensional modeling of the chemical kinetics in low temperature plasmas, for all possible combinations of CO_2, CH_4, N_2, O_2 and H_2O, for a wide variety of applications. It will be useful, for instance, for CO_2 conversion studies in the presence of both CH_4 and N_2, as well as for unravelling the possibilities of plasma-based multi-reforming processes. Furthermore, also in other fields, such as (plasma-assisted) combustion and even more exotic applications, like planetary atmosphere and spacecraft re-entry modeling, this chemistry set could also be used as a foundation to build a comprehensive computational data set.

This comprehensive model was first validated by comparing the calculated CO_2 (and CH_4) conversion for pure CO_2, as well as CO_2/CH_4, CO_2/N_2, CH_4/N_2 and CO_2/H_2O gas mixtures, with experimental data from our earlier work. Subsequently, a more extensive validation was performed by a combined calculation and experimental study, investigating the conversion of CH_4 and CO_2, as well as the selectivity of the major products, in a $CO_2/CH_4/N_2$ mixture, for varying CO_2/CH_4 ratios and N_2 contents, as well as upon O_2 and H_2O addition. Good agreement was reached with the experimental data, indicating that the chemical kinetics model sufficiently captures the underlying plasma chemistry for these processes.

The presence of N_2 in a CO_2/CH_4 gas mixture clearly enhances the absolute CO_2 and CH_4 conversion, due to dissociation of CO_2 and CH_4 upon collision with nitrogen metastable molecules (mainly $N_2(a'\Sigma_u^-)$ and $N_2(a'\Sigma_u^-)$), and it also yields a slight increase in the syngas (H_2/CO) ratio. This is because the N_2 metastable molecules contribute more to the dissociation of CH_4, yielding H_2, due to the higher dissociation rate than that of CO_2. Moreover, at a fixed CH_4 content of 10 %, increasing the CO_2/CH_4 mixing ratio from 0.5 to 4, by modifying the N_2 content, yields a drop in the H_2/CO ratio from 2.45 to 0.42. These results show that we can exert great control over the H_2/CO ratio by changing the mixing ratio.

Although the addition of O_2 is also beneficial for the CH_4 conversion, due to a shift towards POX over DRM, it is accompanied by a severe drop in CO_2 conversion and syngas ratio. Furthermore, a large fraction of the converted CH_4 is transformed into H_2O rather than value-added products.

The addition of H_2O had virtually no effect on the CH_4 and CO_2 conversion. This is interesting, because in a pure CO_2/H_2O mixture, H_2O addition leads to a drop in CO_2 conversion. [73] The reason is that the H atoms, originating from CH_4 dissociation, react with the OH radicals, so that the latter do not recombine with CO into CO_2, which is the limiting process in the CO_2/H_2O mixture. [73] Additionally, the syngas ratio increases due to the effective conversion of H_2O into H_2.

Although this new chemical kinetics model already yields good agreement with experimental data for various gas mixtures and a wide range of mixing ratios, we should remain cautious when using its results—this is true for any model. The chemistry set contains 1729 reactions, each with its corresponding cross section or rate coefficient, which are subject to certain uncertainties. [94] The latter will of course be reflected in the results.

A crucial next step in the field of plasma chemistry modeling should consist of performing a detailed uncertainty analysis and sensitivity studies. By doing so, the impact of these uncertainties on the model predictions can be revealed, and the accuracy of the model can be determined. Such an analysis was presented already for less complicated mixtures, i.e. by Turner for a He/O_2 mixture, [95-97] and in our group for a CO_2 plasma. [38] Although this will be a huge amount of work, we will continue along these lines, since it is indispensable to fully explore the predictive character of such a model.

Additionally, the model presented here mainly applies to a DBD plasma reactor, which has been mostly used for gas conversion studies up to now. However, other types of plasmas are also gaining increasing interest, like microwave plasmas and gliding arc discharges.[11] They operate at somewhat different conditions, such as lower reduced electric field (i.e., ratio of electric field over gas density) around 50 – 100 Td. At these conditions, the electron temperature is in the order of 1 eV, which is most suitable for vibrational excitation. The low vibrational levels will gradually populate higher vibrational levels by vibration-vibration collisions (so-called VV relaxation), and the highest vibrational levels will easily dissociate. Hence, this process of vibrational ladder climbing leading to dissociation is the most energy-efficient process for CO_2 dissociation. This explains why CO_2 dissociation is quite energy efficient in microwave and gliding arc discharges.[4,11] These processes are not considered in detail in the model presented here, as they are of minor importance in a DBD. However, a detailed model for the CO_2 vibrational kinetics has already been developed within the group PLASMANT, [34-35] as well as models for CO_2/N_2 and N_2/O_2 mixtures, accounting in detail for the vibrational kinetics of CO_2, N_2 and O_2.[6,82] In the future, it would be useful to extend this newly developed model for the $CO_2/CH_4/N_2/O_2/H_2O$ mixture with the vibrational kinetics of the various molecules, so that this model becomes applicable to other plasma types as well. This is not only true for the CO_2 vibrational levels, but the N_2 vibrational levels can also be important for CO_2 (and maybe CH_4) dissociation. [82] Furthermore, when the CO_2 conversion is significant, the CO vibrational kinetics should be considered as well, in relation with the formation of C and O atoms. [98] Again, adding the vibrational levels of all these molecules will require major efforts, in view of the possible coupling between all these vibrational levels, and keeping in mind uncertainties in all rate coefficients, [95-97] and the approximations that need to be made. [15-16]

This combined computational and experimental study reveals that the major products formed by mixtures of CO_2, CH_4, N_2, O_2 and H_2O are syngas and some higher hydrocarbons (mainly C_2H_6 and C_3H_8), as well as H_2O, while the concentrations of oxygenates like methanol, formic acid, formaldehyde, as well as hydrogen cyanide, are almost negligible. Hence, to increase the product selectivity of future plasma-based reforming processes, preferably to these oxygenates, combinations with a catalyst or membranes will be necessary. This brings us to another future necessity in the field of plasma chemistry modeling, i.e., the need to extend these models with surface reactions, as recently done for NH_3 synthesis by Hong et al. [99] This step would make it possible for 0D plasma chemistry models to account for plasma catalysis, and thus to make it possible to predict the requirements of the underlying plasmachemical pathways to selectively produce the desired value-added compounds. This stresses the power that lies within this type of modeling studies, i.e. to unravel the underlying chemical pathways to obtain a better understanding of the chemistry taking place, which in turn allows to predict whether new conditions could be more promising, and help to point experiments in the right direction.

ASSOCIATED CONTENT

*S Supporting Information

The Supporting Information is available free of charge on the ACS Publications website at DOI: xx.xxxx/acs.jpcc.xxxxxxx. An overview of the reactions included in the model (PDF)

ACKNOWLEDGMENTS

The authors acknowledge financial support from the European Marie Skłodowska-Curie Individual Fellowship "GlidArc" within Horizon2020 (Grant No. 657304), the Fund for Scientific Research Flanders (FWO) (grant nos G.0217.14N, G.0254.14N and G.0383.16N), Competitive Research Funding from King Abdullah University of Science and Technology (KAUST), the IAP/7 (Inter-university Attraction Pole) program 'PSI-Physical Chemistry of Plasma-Surface Interactions', financially supported by the Belgian Federal Office for Science Policy (BELSPO), as well as the Fund for Scientific Research Flanders (FWO). This work was carried out in part using the Turing HPC infrastructure at the CalcUA core facility of the Universiteit Antwerpen, a division of the Flemish Supercomputer Center VSC, funded by the Hercules Foundation, the Flemish Government (department EWI) and the University of Antwerp.

REFERENCE

(1) Adamovich, I.; Baalrud, S. D.; Bogaerts, A.; Bruggeman, P. J.; Cappelli, M.; Colombo, V.; Czarnetzki, U.; Ebert, U.; Eden, J. G.; Favia, P.; et al. The 2017 Plasma Roadmap: Low Temperature Plasma Science and Technology. *J. Phys. D. Appl. Phys.* **2017**, *50* (32), 323001.

(2) Lee, C. G. N.; Kanarik, K. J.; Gottscho, R. A. The Grand Challenges of Plasma Etching: A Manufacturing Perspective. *J. Phys. D. Appl. Phys.* **2014**, *47* (27), 273001.

(3) Bogaerts, A.; Neyts, E.; Gijbels, R.; van der Mullen, J. Gas Discharge Plasmas and Their Applications, *Spectrochim. Acta, Part B* **2002**, *57*, 609–658.

(4) Fridman, A. *Plasma Chemistry*; Cambridge University Press: New York, 2008.

(5) Chang, J. S. Recent Development of Plasma Pollution Control Technology: A Critical Review. *Sci. & Tech. of Adv. Materials* **2001**, *2*, 571-576.

(6) Wang, W. Z.; Patil, B.; Heijkers, S.; Hessel, V.; Bogaerts, A. Nitrogen Fixation by Gliding Arc Plasma: Better Insight by Chemical Kinetics Modelling. ChemSusChem **2017**, *10*, 2145–2157

(7) Patil, B. S.; Cherkasov, N.; Lang, J.; Ibhadon, A. O.; Hessel, V., Wang, Q. Low Temperature Plasma-Catalytic NOx Synthesis in a Packed DBD Reactor: Effect of Support Materials and Supported Active Metal Oxides. *Appl. Catal. B- Environ.* **2016**, *194*, 123-133.

(8) Chen, H. L.; Lee, H. M.; Chen, S. H.; Chao, Y.; Chang, M. B. Review of Plasma Catalysis on Hydrocarbon Reforming for Hydrogen Production—Interaction, Integration, and Prospects. *Appl. Catal. B: Environ.* **2008**, *85*, 1-9.

(9) Snoeckx, R; Rabinovich, A; Dobrynin, D; Bogaerts, A; Fridman, A. Plasma Based Liquefaction of Methane: the Road from Hydrogen Production to Direct Methane Liquefaction. *Plasma Processes and Polymers* **2017**, *14*, 1600115.

(10) Tu, X.; Whitehead, J. C. Plasma-Catalytic Dry Reforming of Methane in an Atmospheric Dielectric Barrier Discharge: Understanding the Synergistic Effect at Low Temperature. *Appl. Catal. B: Environ.* **2002**, *125*, 439–448.

(11) Snoeckx, R.; Bogaerts, A. Plasma Technology – a Novel Solution for CO_2 Conversion? *Chem. Soc. Rev.* **2017**, *46* (19), 5805–5863.

(12) Neyts, E. C.; Bogaerts, A. Understanding plasma catalysis through modelling and simulation—a review. J. Phys. D: Appl. Phys. **2014**, *47*, 224010.

(13) Neyts, E. C.; Ostrikov, K.; Sunkara, M. K. ; Bogaerts, A. Plasma catalysis: Synergistic effects at the nanoscale. Chem. Rev. **2015**, *115*, 13408-13446.

(14) Whitehead J. C., Plasma–catalysis: the Known Knowns, the Known Unknowns and the Unknown Unknowns. *J. Phys. D: Appl. Phys.* **2016**, *49*, 243001.

(15) Bogaerts, A.; De Bie, C.; Snoeckx, R.; Kozák, T. Plasma Based CO_2 and CH_4 Conversion: A Modeling Perspective. *Plasma Process. Polym.* **2017**, *14* (6), 1600070.

(16) Bogaerts, A.; Berthelot, A.; Heijkers, S.; Kolev, S.; Snoeckx, R.; Sun, S. R.; Trenchev, G.; Van Laer, K.; Wang, W. CO_2 Conversion by Plasma Technology: Insights from Modeling the Plasma Chemistry and Plasma Reactor Design. *Plasma Sources Sci. Technol.* **2017**, *26* (6), 63001.

(17) Zou, J. J.; Zhang, Y. P.; Liu, C. J.; Li, Y.; Eliasson, B. Starch-enhanced Synthesis of Oxygenates from Methane and Carbon Dioxide Using Dielectric-Barrier Discharges. *Plasma Chem. Plasma Process.* **2003**, *23*, 69−82.

(18) Krauss, M.; Eliasson, B.; Kogelschatz, U.; Wokaun, A. CO_2 Reforming of Methane by the Combination of Dielectric-Barrier Discharges and Catalysis. *Phys. Chem. Chem. Phys.* **2001**, *3*, 294−300.

(19) Mei, D. H.; Zhu, X. B. ; He, Y. L.; Yan, J. D.; Tu, X. Plasma-assisted Conversion of CO_2 in A Dielectric Barrier Discharge Reactor: Understanding the Effect of Packing Materials. *Plasma Sources Sci. Technol.* **2015**, *24*(1), 015011.

(20) Tu, X. ; Gallon, H. J. ; Twigg, M. V. ; Gorry, P. A.; Whitehead, J. C. Dry reforming of methane over a NI/AL_2O_3 catalyst in a coaxial dielectric barrier discharge reactor. *J. Phys. D: Appl. Phys.* **2011**, *44*, 274007.

(21) IPCC. *Summary for Policymakers*; 2014.

(22) McDonough, W.; Braungart, M.; Anastas, P. T.; Zimmerman, J. B. Peer Reviewed: Applying the Principles of Green Engineering to Cradle-to-Cradle Design. *Environ. Sci. Technol.* **2003**, *37* (23), 434A–441A.

(23) Jiang, Z.; Xiao, T.; Kuznetsov, V. L.; Edwards, P. P. Turning Carbon Dioxide into Fuel. *Philos. Trans. R. Soc. A Math. Phys. Eng. Sci.* **2010**, *368* (1923), 3343–3364.

(24) Mikkelsen, M.; Jørgensen, M.; Krebs, F. C. The Teraton Challenge. A Review of Fixation and Transformation of Carbon Dioxide. *Energy Environ. Sci.* **2010**, *3* (1), 43–81.

(25) Ju, Y.; Sun, W. T. Plasma Assisted Combustion: Dynamics and Chemistry. *Prog. Energy Combust. Sci.* **2015**, *48*, 21–83.

(26) Starikovskaia, S. M. Plasma-assisted ignition and combustion: nanosecond discharges and development of kinetic mechanisms. *J. Phys. D: Appl. Phys.* **2004**, *47*, 353001.

(27) Gokcen, T. N_2-CH_4-Ar Chemical Kinetic Model for Simulations of Atmospheric Entry to Titan. *J. Thermophys Heat Transfer* **2017**, *21*(1), 9-18

(28) Bultel, A.; Annaloro J. Elaboration of Collisional–Radiative Models for Flows Related to Planetary Entries into the Earth and Mars Atmospheres. *Plasma Sources Sci. Technol.* **2013**, *22*, 025008.

(29) Aerts, R.; Somers, W.; Bogaerts, A. Carbon Dioxide Splitting in a Dielectric Barrier Discharge Plasma: A Combined Experimental and Computational Study. *ChemSusChem* **2015**, *8* (4), 702–716.

(30) Wang, W.; Berthelot, A.; Kolev, S.; Tu, X.; Bogaerts, A. CO_2 Conversion in a Gliding Arc Plasma: 1D Cylindrical Discharge Model. *Plasma Sources Sci. Technol.* **2016**, *25* (6), 65012.

(31) Wang, W.; Mei, D.; Tu, X.; Bogaerts, A. Gliding Arc Plasma for CO_2 Conversion: Better Insights By a Combined Experimental and Modelling Approach. *Chem. Eng. J.* **2017**, *330*, 11-25.

(32) Sun, S. R.; Wang, H. X.; Mei, D. H.; Tu, X.; Bogaerts, A. CO_2 Conversion in a Gliding Arc Plasma: Performance Improvement Based on Chemical Reaction Modeling. *J. CO_2 Util.* **2017**, *17*, 220–234.

(33) Aerts, R.; Martens, T.; Bogaerts, A. Influence of Vibrational States on CO_2 Splitting by Dielectric Barrier Discharges. *J. Phys. Chem. C* **2012**, *116* (44), 23257–23273.

(34) Kozák, T.; Bogaerts, A. Evaluation of the Energy Efficiency of CO_2 Conversion in Microwave Discharges Using a Reaction Kinetics Model. *Plasma Sources Sci. Technol.* **2015**, *24* (1), 15024.

(35) Kozák, T.; Bogaerts, A. Splitting of CO_2 by Vibrational Excitation in Non-Equilibrium Plasmas: A Reaction Kinetics Model. *Plasma Sources Sci. Technol.* **2014**, *23* (4), 45004.

(36) Berthelot, A.; Bogaerts, A. Modeling of Plasma-Based CO_2 Conversion: Lumping of the Vibrational Levels. *Plasma Sources Sci. Technol.* **2016**, *25* (4), 45022.

(37) Berthelot, A.; Bogaerts, A. Modeling of CO_2 Splitting in a Microwave Plasma: How to Improve the Conversion and Energy Efficiency. *J. Phys. Chem. C* **2017**, *121* (15), 8236–8251.

(38) Berthelot, A.; Bogaerts, A. Modeling of CO_2 Plasma: Effect of Uncertainties in the Plasma Chemistry. *Plasma Sources Sci. Technol.* **2017**, *26*, 115002.

(39) Koelman, P.; Heijkers, S.; Tadayon Mousavi, S.; Graef, W.; Mihailova, D.; Kozak, T.; Bogaerts, A.; van Dijk, J. A Comprehensive Chemical Model for the Splitting of CO_2 in Non-Equilibrium Plasmas. *Plasma Process. Polym.* **2017**, *14* (4–5), 1–20.

(40) Ponduri, S.; Becker, M. M.; Welzel, S.; Van De Sanden, M. C. M.; Loffhagen, D.; Engeln, R. Fluid Modelling of CO_2 Dissociation in a Dielectric Barrier Discharge. *J. Appl. Phys.* **2016**, *119* (9).

(41) Pietanza, L. D.; Colonna, G.; D'Ammando, G.; Laricchiuta, A.; Capitelli, M. Non Equilibrium Vibrational Assisted Dissociation and Ionization Mechanisms in Cold CO_2 Plasmas. *Chem. Phys.* **2016**, *468*, 44–52.

(42) Pietanza, L. D.; Colonna, G.; D'Ammando, G.; Laricchiuta, A.; Capitelli, M. Electron Energy Distribution Functions and Fractional Power Transfer In "cold" and Excited CO_2 Discharge and Post Discharge Conditions. *Phys. Plasmas* **2016**, *23* (1).

(43) Pietanza, L. D.; Colonna, G.; Laporta, V.; Celiberto, R.; D'Ammando, G.; Laricchiuta, A.; Capitelli, M. Influence of Electron Molecule Resonant Vibrational Collisions over the Symmetric Mode and Direct Excitation-Dissociation Cross Sections of CO_2 on the Electron Energy Distribution Function and Dissociation Mechanisms in Cold Pure CO_2 Plasmas. *J. Phys. Chem. A* **2016**, *120* (17), 2614–2628.

(44) Pietanza, L. D.; Colonna, G.; D'Ammando, G.; Capitelli, M. Time-Dependent Coupling of Electron Energy Distribution Function, Vibrational Kinetics of the Asymmetric Mode of CO_2 and Dissociation, Ionization and Electronic Excitation Kinetics under Discharge and Post-Discharge Conditions. *Plasma Phys. Control. Fusion* **2017**, *59* (1), 14035.

(45) Pietanza, L. D.; Colonna, G.; D'Ammando, G.; Laricchiuta, a; Capitelli, M. Vibrational Excitation and Dissociation Mechanisms of CO_2 under Non-Equilibrium Discharge and Post-Discharge Conditions. *Plasma Sources Sci. Technol.* **2015**, *24* (4), 42002.

(46) Capitelli, M.; Colonna, G.; D'Ammando, G.; Hassouni, K.; Laricchiuta, A.; Pietanza, L. D. Coupling of Plasma Chemistry, Vibrational Kinetics, Collisional-Radiative Models and Electron Energy Distribution Function Under Non-Equilibrium Conditions. *Plasma Process. Polym.* **2017**, *14* (1–2), 1600109.

(47) Moss, M. S.; Yanallah, K.; Allen, R. W. K.; Pontiga, F. An Investigation of CO_2 Splitting Using Nanosecond Pulsed Corona Discharge: Effect of Argon Addition on CO_2 Conversion and Energy Efficiency. *Plasma Sources Sci. Technol.* **2017**, *26* (3), 35009.

(48) Cheng, J.-L.; Wang, H.-X.; Sun, S.-R. Analysis of Dissociation Mechanism of CO_2 in a Micro-Hollow Cathode Discharge. *Chinese Phys. Lett.* **2016**, *33* (10), 108201.

(49) de la Fuente, J. F.; Moreno, S. H.; Stankiewicz, A. I.; Stefanidis, G. D. A New Methodology for the Reduction of Vibrational Kinetics in Non-Equilibrium Microwave Plasma: Application to CO_2 Dissociation. *React. Chem. Eng.* **2016**, *1* (5), 540–554.

(50) Indarto, A.; Choi, J.; Lee, H.; Song, H. K. Kinetic Modeling of Plasma Methane Conversion Using Gliding Arc. *J. Nat. Gas Chem.* **2005**, *14*, 13–21.

(51) Indarto, A.; Coowanitwong, N.; Choi, J. W.; Lee, H.; Song, H. K. Kinetic Modeling of Plasma Methane Conversion in a Dielectric Barrier Discharge. *Fuel Process. Technol.* **2008**, *89* (2), 214–219.

(52) De Bie, C.; Verheyde, B.; Martens, T.; van Dijk, J.; Paulussen, S.; Bogaerts, A. Fluid Modeling of the Conversion of Methane into Higher Hydrocarbons in an Atmospheric Pressure Dielectric Barrier Discharge. *Plasma Process. Polym.* **2011**, *8* (11), 1033–1058.

(53) Yang, Y. Direct Non-Oxidative Methane Conversion by Non-Thermal Plasma: Modeling Study. *Plasma Chem. Plasma Process.* **2003**, *23* (2), 327–346.

(54) Luche, J.; Aubry, O.; Khacef, A.; Cormier, J.-M. Syngas Production from Methane Oxidation Using a Non-Thermal Plasma: Experiments and Kinetic Modeling. *Chem. Eng. J.* **2009**, *149* (1–3), 35–41.

(55) Zhou, L. M.; Xue, B.; Kogelschatz, U.; Eliasson, B. Nonequilibrium Plasma Reforming of Greenhouse Gases to Synthesis Gas. *Energy & Fuels* **1998**, *12* (6), 1191–1199.

(56) Machrafi, H.; Cavadias, S.; Amouroux, J. Valorization by Means of Dielectric Barrier Discharge. *J. Phys. Conf. Ser.* **2011**, *275*, 12016.

(57) Goujard, V.; Tatibouët, J. M.; Batiot-Dupeyrat, C. Carbon Dioxide Reforming of Methane Using a Dielectric Barrier Discharge Reactor: Effect of Helium Dilution and Kinetic Model. *Plasma Chem. Plasma Process.* **2011**, *31* (2), 315–325.

(58) Wang, J. G.; Liu, C. J.; Eliassion, B. Density Functional Theory Study of Synthesis of Oxygenates and Higher Hydrocarbons from Methane and Carbon Dioxide Using Cold Plasmas. *Energy & Fuels* **2004**, *18* (1), 148–153.

(59) Istadi, I.; Amin, N. A. S. Modelling and Optimization of Catalytic-Dielectric Barrier Discharge Plasma Reactor for Methane and Carbon Dioxide Conversion Using Hybrid Artificial Neural Network-Genetic Algorithm Technique. *Chem. Eng. Sci.* **2007**, *62* (23), 6568–6581.

(60) Kraus, M.; Egli, W.; Haffner, K.; Eliasson, B.; Kogelschatz, U.; Wokaun, A. Investigation of Mechanistic Aspects of the Catalytic CO_2 Reforming of Methane in a Dielectric-Barrier Discharge Using Optical Emission Spectroscopy and Kinetic Modeling. *Phys. Chem. Chem. Phys.* **2002**, *4* (4), 668–675.

(61) Liu, C.-J.; Li, Y.; Zhang, Y.-P.; Wang, Y.; Zou, J.; Eliasson, B.; Xue, B. Production of Acetic Acid Directly from Methane and Carbon Dioxide Using Dielectric-Barrier Discharges. *Chem. Lett.* **2001**, *30* (12), 1304–1305.

(62) Janeco, A.; Pinha, N. R.; Guerra, V. Electron Kinetics in He / CH_4 / CO_2 Mixtures Used for Methane Conversion. *J. Phys. Chem. C* **2015**, *119*, 109.

(63) Snoeckx, R.; Aerts, R.; Tu, X.; Bogaerts, A. Plasma-Based Dry Reforming: A Computational Study Ranging from the Nanoseconds to Seconds Time Scale. *J. Phys. Chem. C* **2013**, *117* (10), 4957–4970.

(64) Snoeckx, R.; Zeng, Y. X.; Tu, X.; Bogaerts, A. Plasma-Based Dry Reforming: Improving the Conversion and Energy Efficiency in a Dielectric Barrier Discharge. *RSC Adv.* **2015**, *5* (38), 29799–29808.

(65) De Bie, C.; Martens, T.; van Dijk, J.; Paulussen, S.; Verheyde, B.; Corthals, S.; Bogaerts, A. Dielectric Barrier Discharges Used for the Conversion of Greenhouse Gases: Modeling the Plasma Chemistry by Fluid Simulations. *Plasma Sources Sci. Technol.* **2011**, *20* (2), 24008.

(66) De Bie, C.; Van Dijk, J.; Bogaerts, A. The Dominant Pathways for the Conversion of Methane into Oxygenates and Syngas in an Atmospheric Pressure Dielectric Barrier Discharge. *J. Phys. Chem. C* **2015**, *119* (39), 22331–22350.

(67) Zhou, L. M.; Xue, B.; Kogelschatz, U.; Eliasson, B. Partial Oxidation of Methane to Methanol with Oxygen or Air in a Nonequilibrium Discharge Plasma. *Plasma Chem. Plasma Process.* **1998**, *18* (3), 375–393.

(68) Nair, S. A.; Nozaki, T.; Okazaki, K. Methane Oxidative Conversion Pathways in a Dielectric Barrier Discharge Reactor-Investigation of Gas Phase Mechanism. *Chem. Eng. J.* **2007**, *132* (1–3), 85–95.

(69) Goujard, V.; Nozaki, T.; Yuzawa, S.; Ağiral, A.; Okazaki, K. Plasma-Assisted Partial Oxidation of Methane at Low Temperatures: Numerical Analysis of Gas-Phase Chemical Mechanism. *J. Phys. D. Appl. Phys.* **2011**, *44* (27), 274011.

(70) Nozaki, T.; Aĝiral, A.; Yuzawa, S.; Han Gardeniers, J. G. E.; Okazaki, K. A Single Step Methane Conversion into Synthetic Fuels Using Microplasma Reactor. *Chem. Eng. J.* **2011**, *166* (1), 288–293.

(71) Zhou, J.; Xu, Y.; Zhou, X.; Gong, J.; Yin, Y.; Zheng, H.; Guo, H. Direct Oxidation of Methane to Hydrogen Peroxide and Organic Oxygenates in a Double Dielectric Plasma Reactor. *ChemSusChem* **2011**, *4* (8), 1095–1098.

(72) Matin, N. S.; Whitehead, J. C. A Chemical Model for the Atmospheric Pressure Plasma Reforming of Methane with Oxygen. In *28th ICPIG*; 2007; pp 983–986.

(73) Snoeckx, R.; Ozkan, A.; Reniers, F. ; Bogaerts, A. The Quest for Value-Added Products from Carbon Dioxide and Water in a Dielectric Barrier Discharge: a Chemical Kinetics Study. *ChemSusChem* **2017**, *10*(2), 409–424.

(74) De Bie, C.; Van Dijk, J.; Bogaerts, A. CO_2 Hydrogenation in a Dielectric Barrier Discharge Plasma Revealed. *J. Phys. Chem. C* **2016**, *120* (44), 25210–25224.

(75) Ding, K.; Lieberman, Reaction pathways for Bio-Active Species in a He/H_2O Atmospheric Pressure Capacitive Discharge. *J. Phys. D: Appl. Phys.* **2015**, *48*, 035401.

(76) Legrand, J. C.; Diamy, A. M.; Hrach, R.; Hrachova, V. Kinetics of Reactions in CH_4/N_2 Afterglow Plasma. *Vacuum* **1997**, *48* (7–9), 671–675.

(77) Majumdar, A.; Behnke, J. F.; Hippler, R.; Matyash, K.; Schneider, R. Chemical Reaction Studies in CH_4/Ar and CH_4/N_2 Gas Mixtures of a Dielectric Barrier Discharge. *J. Phys. Chem. A* **2005**, *109* (41), 9371–9377.

(78) Pintassilgo, C. D.; Jaoul, C.; Loureiro, J.; Belmonte, T.; Czerwiec, T. Kinetic Modelling of a N_2 Flowing Microwave Discharge with CH_4 Addition in the Post-Discharge for Nitrocarburizing Treatments. *J. Phys. D. Appl. Phys.* **2007**, *40* (12), 3620–3632.

(79) Jauberteau, J. L.; Jauberteau, I.; Cinelli, M. J.; Aubreton, J. Reactivity of Methane in a Nitrogen Discharge Afterglow. *New J. Phys.* **2002**, *4*, 39.

(80) Savinov, S. Y.; Lee, H.; Song, H. K.; Na, B. K. The Effect of Vibrational Excitation of Molecules on Plasmachemical Reactions Involving Methane and Nitrogen. *Plasma Chem. Plasma Process.* **2003**, *23* (1), 159–173.

(81) Snoeckx, R.; Setareh, M.; Aerts, R.; Simon, P.; Maghari, A.; Bogaerts, A. Influence of N_2 Concentration in a CH_4/N_2 Dielectric Barrier Discharge Used for CH_4 Conversion into H_2. *Int. J. Hydrogen Energy* **2013**, *38* (36), 16098–16120.

(82) Heijkers, S.; Snoeckx, R.; Kozák, T.; Silva, T.; Godfroid, T.; Britun, N.; Snyders, R.; Bogaerts, A. CO_2 Conversion in a Microwave Plasma Reactor in the Presence of N_2 : Elucidating the Role of Vibrational Levels. *J. Phys. Chem. C* **2015**, *119* (23), 12815–12828.

(83) Snoeckx, R.; Heijkers, S.; Van Wesenbeeck, K.; Lenaerts, S.; Bogaerts, A. CO_2 Conversion in a Dielectric Barrier Discharge Plasma: N_2 in the Mix as a Helping Hand or Problematic Impurity? *Energy Environ. Sci.* **2016**, *9* (3), 999–1011.

(84) Zhang, X.; Cha, M. S. Electron-Induced Dry Reforming of Methane in a Temperature-Controlled Dielectric Barrier Discharge Reactor. *J. Phys. D. Appl. Phys.* **2013**, *46* (41), 415205.

(85) Zhang, X.; Cha, M. S. Partial Oxidation of Methane in a Temperature-Controlled Dielectric Barrier Discharge Reactor. *Proc. Combust. Inst.* **2015**, *35* (3), 3447–3454.

(86) van Dijk, J.; Kroesen, G.M.W. ; and Bogaerts A., Plasma Modeling and Numerical Simulation. *J. Phys. D: Appl. Phys.* **2009**, *42*, 190301.

(87) Bogaerts, A.; Alves, L.L. Special Issue on Numerical Modeling of Low-Temperature Plasmas for Various Applications – Part I: Review and Tutorial Papers on Numerical Modeling Approaches. *Plasma Process. Polym.* **2017**, *14*, 169011.

(88) Alves, L.L.; Bogaerts, A.; Guerra, V.; Turner, M. M. Foundations of Modelling of Low-Temperature Plasmas. *Plasma Sources Sci. Technol.*, 2017, in press.

(89) Van Gaens, W.; Bogaerts, A. Kinetic Modelling for an Atmospheric Pressure Argon Plasma Jet in Humid Air. *J. Phys. D. Appl. Phys.* **2013**, *46*, 275201.

(90) Zhou, L. M.; Xue, B.; Kogelschatz, U.; Eliasson, B. Nonequilibrium Plasma Reforming of Greenhouse Gases to Synthesis Gas. *Energ. Fuel.* **1998**, *12*, 1191-1199.

(91) Zhang, K.; Kogelschatz, U.; Eliasson, B. Conversion of Greenhouse Gases to Synthesis Gas and Higher Hydrocarbons. *Energ. Fuel.* **2001**, *15*, 395-402.

(92) Aerts, R.; Snoeckx, R.; Bogaerts, A. In-Situ Chemical Trapping of Oxygen in the Splitting of Carbon Dioxide by Plasma. *Plasma Process. Polym.* **2014**, *11*, 985–994.

(93) Atkins, P.W. (1993). The Elements of Physical Chemistry (3rd ed.). Oxford University Press.

(94) Bogaerts, A.; Wang, W. Z.; Berthelot A.; Guerra, V. Modeling Plasma-based CO_2 Conversion: Crucial Role of the Dissociation Cross Section. *Plasma Sources Sci. Technol.* **2016**, *25*, 055016.

(95) Turner, M. M. Uncertainty and Error in Complex Plasma Chemistry Models. *Plasma Sources Sci. Technol.* **2015**, *24*, 035027.

(96) Turner, M. M. Uncertainty and Sensitivity Analysis in Complex Plasma Chemistry Models. *Plasma Sources Sci. Technol.* **2016**, *25*, 015003.

(97) Turner, M. M. Computer Simulation in Low-Temperature Plasma Physics: Future Challenges. *Plasma Process. Polym.* **2017**, *14*, 1600121.

(98) Pietanza, L. D.; Colonna G. and Capitelli M. Non-equilibrium plasma kinetics of reacting CO: an improved state to state approach. *Plasma Sources Sci. Technol.* **2017**, 26, 125007.

(99) Hong, J.; Pancheshnyi, S.; Tam, E.; Lowke, J. J.; Prawer, S.; Murphy, A. B. Kinetic Modelling of NH_3 Production in N_2–H_2 Non-Equilibrium Atmospheric-Pressure Plasma Catalysis. *J. Phys. D: Appl. Phys.* **2017**, *50*, 154005.

TOC GRAPHIC

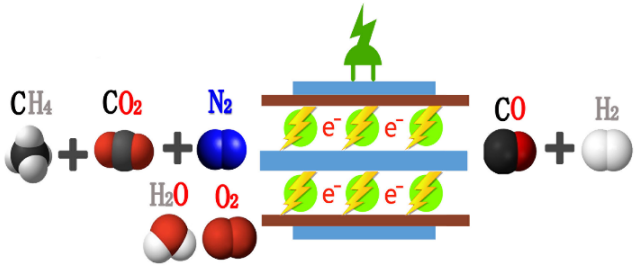

BIOGRAPHIES

Weizong Wang was born in Shandong, China, in 1984. He received double Ph.D. degrees in electrical engineering from Xi'an Jiaotong University, China and University of Liverpool, United Kingdome, in 2013. Since that, he worked at Qian Xuesen Laboratory of Space Technology in China up to 2015, focusing on plasma propulsion. Currently, he is working in the PLASMANT research group at the University of Antwerp in Belgium supported by the Marie Skłodowska-Curie Individual Fellowship towards a better understanding of plasma-based gases conversion into value added products. His main interests concern the fundamental physics, chemistry and applications of low temperature plasmas.

Ramses Snoeckx, born in 1988, obtained master's degrees in both environmental science and chemistry. Combining these specializations, he successfully obtained a PhD in chemistry (2017, University of Antwerp) for his research on plasma-based conversion of greenhouse gases into value-added chemicals and fuels. Currently he's working as postdoctoral fellow at the King Abdullah University of Science and Technology (KAUST). The underlying chemical reactions taking place in plasmas are his prime focus. By relying on a combination of modelling and experimental techniques, he aims to gain the necessary insights in the plasmachemical pathways to improve existing—as well as to find new—applications for plasma-based environmental and energy solutions.

Xuming Zhang was born in Hangzhou, China, in 1981. He received Ph.D. degree from Zhejiang University, China, in 2011. He served in King Abdullah University of Science and Technology (KAUST), as a post-doctoral research fellow from 2011 to 2015. He has been with Zhejiang Gongshang University as an assistant professor since 2016. Dr. Zhang has authored over 30 publications in peer-reviewed journals. His current research interests include non-thermal plasma generation and plasma-induced fuel reforming and environmental remediation.

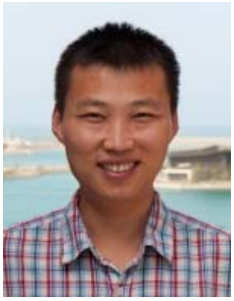

Min Suk Cha was born in Seoul, Korea, in 1970. He received Ph. D. degrees in Mechanical Engineering from Seoul National University in 1999, specialized in Combustion Science. He worked in Korea Institute of Machinery & Materials (KIMM), where he obtained a plasma background, as a Principal Research Scientist from 2000 to 2010. Currently he is Associate Professor in King Abdullah University of Science and Technology (KAUST). His current research interests include plasma (and electrically) assisted combustion, plasma fuel reforming, and in-liquid plasma generations.

Annemie Bogaerts, born in 1971, obtained her PhD in chemistry in 1996, from the University of Antwerp in Belgium. She became professor of physical chemistry in 2003, at this university, and is full professor since 2012. She is head of the interdisciplinary research group PLASMANT. The research activities of her group include modelling of plasma chemistry, plasma reactor design and plasma-surface interactions, as well as plasma experiments, for various applications, including environmental and medical applications (mainly cancer treatment), as well as nanotechnology and analytical chemistry. In recent years, special attention is given to CO_2 conversion by plasma and plasma catalysis.